Chapter 9

Evaluation of Satellite Leaf Area Products

Yan et al.

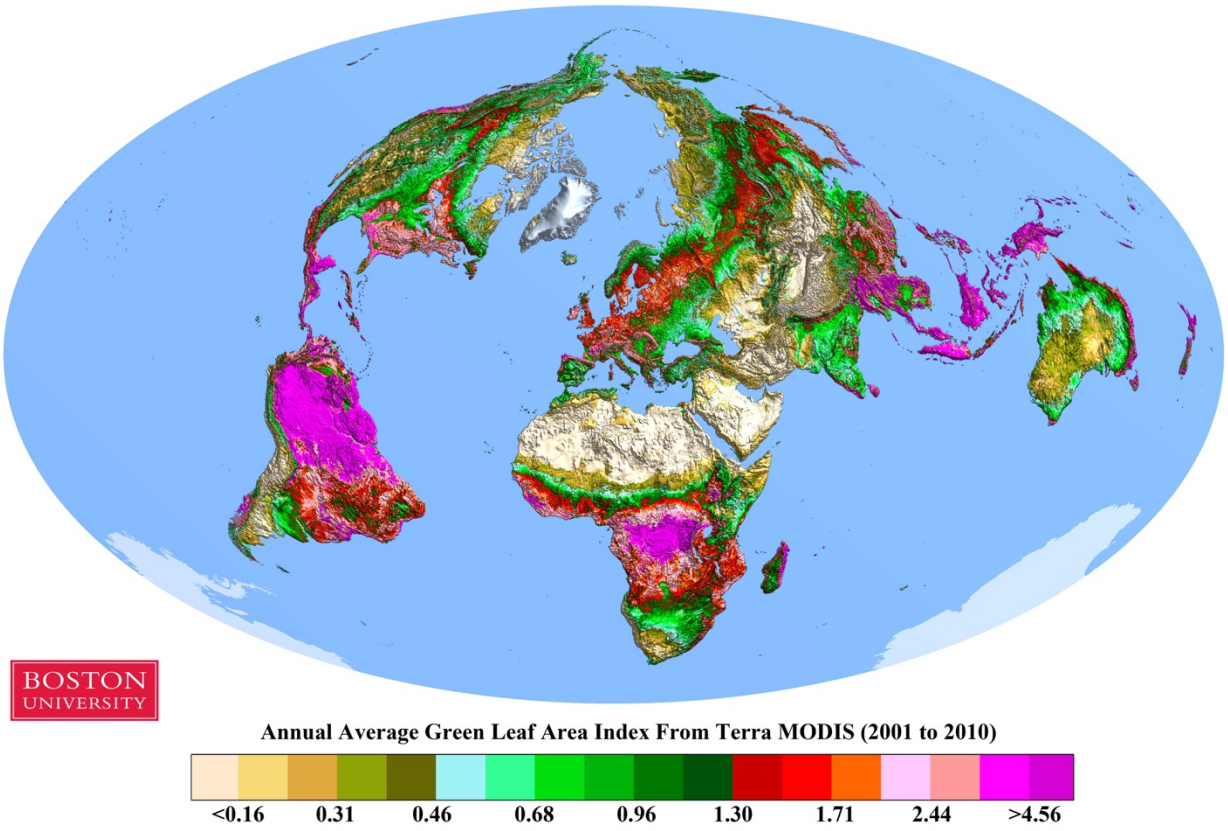

remote sensing

MDPI

Article

Evaluation of MODIS LAI/FPAR Product Collection 6. Part 1: Consistency and Improvements

Kai Yan [1,2,*], Taejin Park [2,*], Guangjian Yan [1], Chi Chen [2], Bin Yang [2,3], Zhao Liu [2], Ramakrishna R. Nemani [4], Yuri Knyazikhin [2] and Ranga B. Myneni [2]

1 School of Geography, State Key Laboratory of Remote Sensing Science, Beijing Normal University, Beijing 100875, China; gjyan@bnu.edu.cn
2 Department of Earth and Environment, Boston University, Boston, MA 02215, USA; chenchi@bu.edu (C.C.); ybjason@bu.edu (B.Y.); liuzhaofairy@gmail.com (Z.L.); jknjazi@bu.edu (Y.K.); ranga.myneni@gmail.com (R.B.M.)
3 Beijing Key Lab of Spatial Information Integration & Its Applications, Institute of RS & GIS, Peking University, Beijing 100871, China
4 NASA Ames Research Center, Moffett Field, CA 94035, USA; rama.nemani@nasa.gov
* Correspondence: kaiyan.earthscience@gmail.com (K.Y.); taejin1392@gmail.com (T.P.); Tel.: +86-186-1001-1902 (K.Y.); +1-617-893-1988 (T.P.)

Academic Editors: Sangram Ganguly, Compton Tucker, Clement Atzberger and Prasad S. Thenkabail
Received: 7 March 2016; Accepted: 20 April 2016; Published: 26 April 2016

Abstract: As the latest version of Moderate Resolution Imaging Spectroradiometer (MODIS) Leaf Area Index (LAI) and Fraction of Photosynthetically Active Radiation (FPAR) products, Collection 6 (C6) has been distributed since August 2015. This collection is evaluated in this two-part series with the goal of assessing product accuracy, uncertainty and consistency with the previous version. In this first paper, we compare C6 (MOD15A2H) with Collection 5 (C5) to check for consistency and discuss the scale effects associated with changing spatial resolution between the two collections and benefits from improvements to algorithm inputs. Compared with C5, C6 benefits from two improved inputs: (1) L2G–lite surface reflectance at 500 m resolution in place of reflectance at 1 km resolution; and (2) new multi-year land-cover product at 500 m resolution in place of the 1 km static land-cover product. Global and seasonal comparison between C5 and C6 indicates good continuity and consistency for all biome types. Moreover, inter-annual LAI anomalies at the regional scale from C5 and C6 agree well. The proportion of main radiative transfer algorithm retrievals in C6 increased slightly in most biome types, notably including a 17% improvement in evergreen broadleaf forests. With same biome input, the mean RMSE of LAI and FPAR between C5 and C6 at global scale are 0.29 and 0.091, respectively, but biome type disagreement worsens the consistency (LAI: 0.39, FPAR: 0.102). By quantifying the impact of input changes, we find that the improvements of both land-cover and reflectance products improve LAI/FPAR products. Moreover, we find that spatial scale effects due to a resolution change from 1 km to 500 m do not cause any significant differences.

Keywords: Leaf Area Index (LAI); Fraction of Photo-synthetically Active Radiation (FPAR); MODIS; Collection 6; evaluation; consistency

1. Introduction

The launch of NASA's Terra and Aqua satellites began a new era in remote sensing of Earth's atmosphere, oceans and land surface. On board these platforms, the MODerate resolution Imaging Spectroradiometer (MODIS) instrument successfully started production and distribution of a variety of products of Earth system parameters [1]. Among these parameters, Leaf Area Index (LAI) and Fraction of Photosynthetically Active Radiation (0.4–0.7 μm) absorbed by vegetation (FPAR) play an important

role in most global models of climate, hydrology, biogeochemistry, and ecosystem productivity by characterizing vegetation canopy structure and energy absorption capacity [2,3].

To take full advantage of MODIS's multi-angular and multi-spectral observation ability, a physical algorithm based on Radiative Transfer (RT) was developed for generating MODIS LAI/FPAR products (MOD15) [4,5]. The MODIS science team aims to provide users with better products by updating product cohorts that are called collections. Since the launch of Terra in December 1999, MODIS land data records have been reprocessed four times. Having stage one validation status, Collection 3 (C3) is the first release of MODIS LAI/FPAR products and covered the period of November 2000 to December 2002. The product accuracy of this version has been estimated using ground measurements obtained from some field campaigns [6]. Collection 4 (C4) covered the period from February 2000 to December 2006 and benefited from the improved inputs and updated look-up-tables (LUTs) [7]. Aimed at reducing the impact of environmental conditions and temporal compositing period, Collection 5 (C5) combined Terra- and Aqua-MODIS sensor data and generated four LAI/FPAR products from February 2000 to present [8]. In addition, C5 used a static 8-biome land-cover map instead of previous 6-biome one. Algorithm refinements were carried out over all biomes but with a major focus on woody vegetation for which a new stochastic RT model was utilized [9].

Collection 6 (C6) represents the latest version and contains the entire time series from February 2000 to the present. This version has been released and distributed free of charge to the public since August 2015 and is expected to benefit from improvements to upstream inputs of the LAI/FPAR algorithm. Before being released, LAI and FPAR products should go through three procedures—algorithm development, product analysis, and validation [8]. Since C6 inherits the same algorithm from C5, we focus on the last two steps and document them in this two-paper series. Product analysis includes assessment of algorithm performance, version consistency and product uncertainty caused by errors in input data [6–8,10]. A check of the consistency between different versions of products is a good way to make sure that there are no theoretical or artificial errors (bugs) in computing code. Moreover, products users should be aware of the improvements in a new version. In this paper, we compare C6 with C5 to check for consistency in terms of spatial distribution, seasonal variations, inter-annual anomalies and spatial coverage. The impact on algorithm retrievals due to changes in inputs is also investigated. Product validation includes direct validation using field measurements, indirect validation using other related parameters such as climatic variables, and inter-comparison with other existing products [11–14]. This part is described in the second paper.

This paper is organized as follows. Section 2 briefly reviews the MODIS LAI/FPAR algorithm and documents improvements seen in C6. Section 3 details the consistency between C6 and C5 along four fronts. Section 4 demonstrates the benefits from improved land-cover and reflectance products that are inputs to the algorithm. A simulation experiment about scale effects is also presented in this section. Concluding remarks are presented in Section 5.

2. MODIS LAI/FPAR Products

2.1. Algorithm Theoretical Description

The operational MODIS LAI/FPAR algorithm consists of a main algorithm that is based on the three-dimensional radiative transfer (3D RT) equation. By describing the photon transfer process, this algorithm links surface spectral bi-directional reflectance factors (BRFs) to both structural and spectral parameters of the vegetation canopy and soil [15,16]. Given atmosphere-corrected BRFs and their uncertainties, the algorithm finds candidates of LAI and FPAR by comparing observed and modeled BRFs that are stored in biome type specific LUTs. All canopy/soil patterns for which observed and modeled BRFs differ within biome-specified thresholds of uncertainties (e.g., 30% and 15% for red and near-infrared bands, respectively, for forest biomes) are considered candidate solutions and the mean values of LAI and FPAR from these solutions are reported as outputs. The law of energy conservation and the theory of spectral invariance are two important features of this main algorithm. The detailed

theoretical basis of the algorithm and implementation aspects are documented in references [1,5,17]. The main algorithm may fail to localize a solution if uncertainties of input BRFs are larger than threshold values or due to deficiencies of the RT model that result in incorrect simulated BRFs. In such case, a back-up empirical method based on relations between the Normalized Difference Vegetation Index (NDVI) and LAI/FPAR [4,18] is utilized to output LAI/FPAR with relatively poor quality—this is called the backup algorithm.

2.2. Algorithm Inputs

Theoretically, the MODIS algorithm can make use of multiple atmosphere-corrected BRFs and their uncertainties. Currently, the MODIS algorithm only utilizes daily surface reflectance at red (648 nm) and near-infrared (858 nm) bands because of high uncertainties in other bands [19]. The uncertainty of input BRFs from the calibration and atmospheric correction process will propagate into the products even if the science algorithm is sound. As critical information, reflectance uncertainties as well as model uncertainties are incorporated to set the threshold of difference between observed and modeled BRFs [5]. Another important input is the biome map, in which global vegetation is classified into eight biomes with different canopy and soil patterns (Figure S1). The eight biomes are: (B1) grasses and cereal crops; (B2) shrubs; (B3) broadleaf crops; (B4) savannas; (B5) evergreen broadleaf forests; (B6) deciduous broadleaf forests; (B7) evergreen needleleaf forests and (B8) deciduous needleleaf forests. With simplifying assumptions and standard constants (e.g., vegetation and soil optical properties) which are assumed to vary with biome and soil types only, using a biome map as prior-knowledge can reduce the number of unknowns of the "ill-posed" inverse problem [1,20].

2.3. Temporal Compositing and Quality Control

Figure 1 shows the flow of MODIS LAI/FPAR C6 production. The algorithm ingests MODIS daily red and near-infrared (NIR) BRFs and a biome map to generate daily LAI/FPAR retrievals without pre-quality-control on inputs. A temporal compositing approach is used to select the best retrievals and generate 8-day or 4-day products from daily retrievals. The compositing algorithm is a two-step scheme: (1) the retrievals are selected according to algorithm path: main algorithm retrievals have the highest priority, and if none are available, back-up algorithm retrievals are selected; (2) the LAI value is selected based on maximum FPAR value [8]. Compositing reduces the impact of day-to-day artificial variations in surface reflectance that are due to cloud and residual atmospheric effects and it is effective in removing contaminated retrievals. As well as LAI/FPAR values, MODIS products store the corresponding quality control (QC) data layers and the users are advised to consult the quality flags when using these products [7]. The key indicator of the quality of retrievals is the algorithm path, which distinguishes the following five categories: (1) main algorithm without saturation; (2) main algorithm with saturation; (3) back-up algorithm due to bad geometry; (4) back-up algorithm due to other problems; and (5) not produced. In addition to algorithm path, the QC layer provides information about presence of clouds, aerosols, and snow, inherited from input reflectance products.

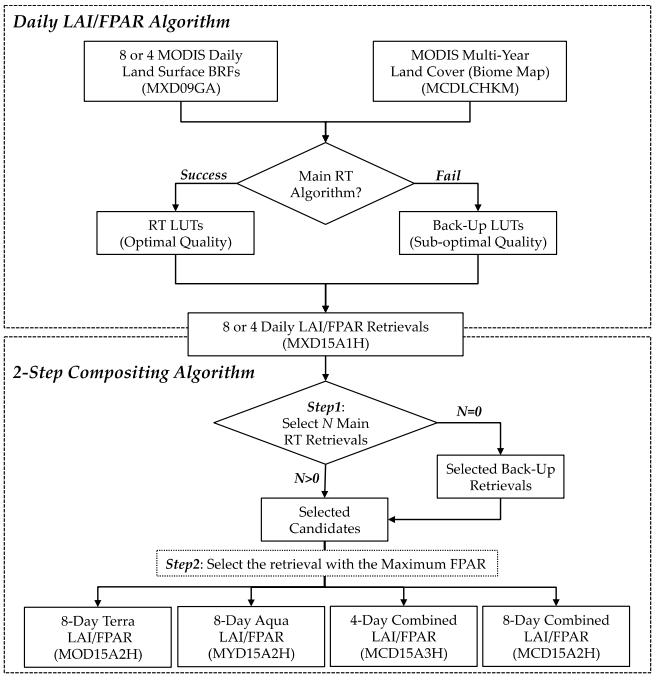

Figure 1. Algorithm flow of MODIS LAI/FPAR Collection 6 production. Four different global products with different compositing (8-day or 4-day) periods and sensor platform combinations (Terra and/or Aqua) are available.

2.4. Improvements of Collection 6

MODIS LAI/FPAR C6 uses the same science algorithm and LUTs as C5. However, this new version can still benefit from improved inputs as discussed below. As the only two inputs, the intermediate data at 1 km resolution of surface reflectances and biome map are replaced by their 500 m version, thus enabling the C6 LAI/FPAR products to have half-kilometer spatial resolution. The significance of this upgrade is two-fold. First, downstream land surface models can benefit from this finer resolution LAI/FPAR products. Second, the LAI/FPAR algorithm uses biome type classification to reduce unknown parameters and each pixel is assumed to belong to only one biome type with some pre-set structural and optical parameters. This assumption is more likely to be satisfied at finer resolutions because of the higher heterogeneity in coarse pixels [21]. Moreover, the smaller pixel ground coverage can reduce the scale gap between remote sensing pixels and ground point measurements, which will reduce uncertainties and human labor during the process of products validation using ground measurements [6,22].

The new version of publicly available MODIS daily surface reflectances (MOD09GA C6) is used to replace the previous intermediate dataset (MODAGAGG) which was generated by aggregating four MOD09GA C5 pixels [23]. This makes it possible for the community to test their own LAI/FPAR algorithms and compare with MODIS products. Improved aerosol retrieval and correction algorithm are employed in the generation of MOD09GA C6 dataset. Moreover, BRDF database is used to better constrain the thresholds used in the snow/cloud detection algorithm. MODIS land-cover product C5 (as input for LAI/FPAR C6) is also reported to be significantly improved through algorithm refinement and input data revise. Comparison of C5 land-cover with C4 (as input for LAI/FPAR C5) showed substantial differences. Cross-validation accuracy assessment indicates an overall accuracy of 75% in C5 land-cover product [24]. In addition, C6 LAI/FPAR replaced the static land-cover input with new multi-year land-cover maps generated with three years of C5 land-cover data. Compared with the previous static land-cover, this new biome type source has a three-year temporal resolution and thus can capture the dynamic changes of biome types. According to previous experience [1,7], C6 LAI/FPAR products can benefit from the improved upstream reflectance and land-cover products [25].

3. Consistency between C5 and C6 LAI/FPAR Products

Good consistency between different product versions creates confidence in LAI/FPAR data sets in both product producers and users, while poor consistency such as large differences diverts attention away from both of them. In this paper, we study the consistency between C5 and C6 along four fronts as discussed below. Note that, except for Sections 3.1 and 3.4 we only focus on the retrievals from the main algorithm.

3.1. Global Distribution

The spatial distribution of LAI and FPAR over the globe during two 8-day composite periods in January and July in the year 2003 are shown in Figure 2a,d and Figure S2. For both LAI and FPAR, there is no visually distinguishable difference between C5 and the new C6. The products from two collections exhibit similar spatial patterns. FPAR shows a similar distribution pattern to LAI, which can be explained by radiative transfer theory [1]. The LAI patterns closely coincide with the biome type distribution (Figure S1)—high LAI over forests and low LAI over herbaceous vegetation. As expected, tropical evergreen forests (e.g., amazon rain forests) have high LAI values (up to 7); somewhat less green are the middle latitude broadleaf forests (e.g., eastern United States). Except bare land and deserts, regions covered by grasses and shrubs generally have low LAI values. The globe looks greener in boreal summer time because of ample illumination conditions over the northern hemisphere, which has greater land surface.

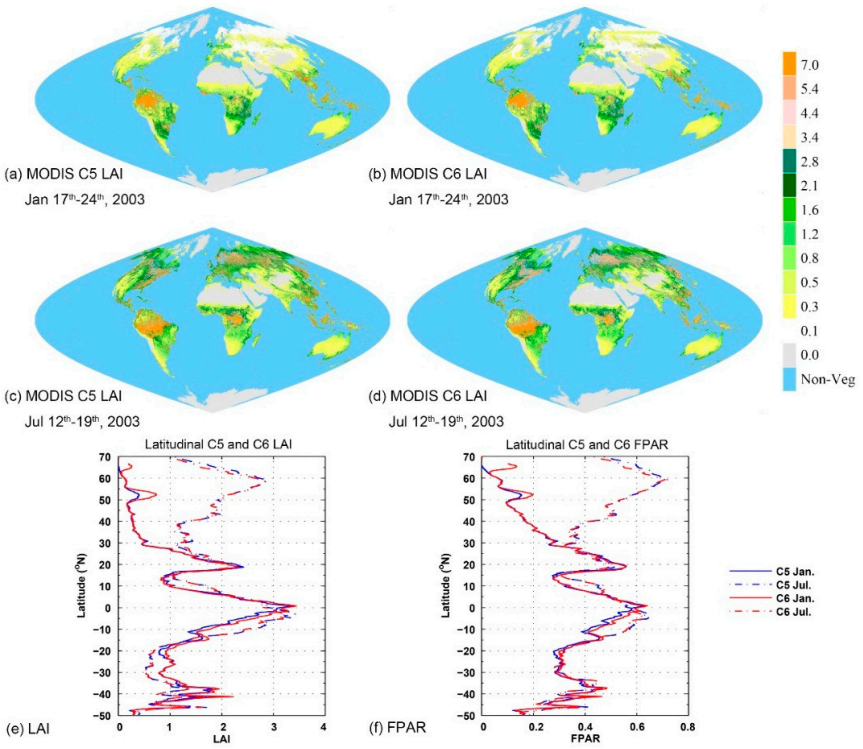

Figure 2. Global distribution of LAI/FPAR from January (17–24 January) and July (12–19 July) of 2003. Panel (**a**–**d**) are color-coded maps of MODIS C6 and C5 LAI. Figure S2 shows FPAR. Area-equal sinusoidal projection is used here; panels (**e**,**f**) show the latitudinal distribution of global LAI and FPAR, respectively. The latitude interval is 0.1°. In these plots, MODIS C6 and C5 use red and blue lines, respectively. Solid and dashed lines depict January and July, respectively.

Figure 2e,f compare the zonal mean LAI and FPAR values from C5 and C6 in January and July. For both LAI and FPAR, the profiles derived from C6 and C5 products match well at most latitude bands

and show consistent latitudinal distribution of LAI and FPAR values. There are two obvious peaks in the tropics (23°N–23°S) which can be explained by the dense vegetation coverage in the three tropical rainforests (South America, Africa and Southeast Asia). As illumination is ample, there is no obvious seasonal difference in these latitude bands. In the higher latitudes, the northern hemisphere shows clear seasonal difference than the southern hemisphere. This is because the dominant biome types in the southern hemisphere are savannas, shrubs and grasses that have smaller seasonal variations than the forests that dominate the northern hemisphere [26] (see Figure S1). We also notice that C5 underestimates C6 in the bands 50°N–55°N and 63°N–70°N. This is caused by changes in input biome type and will be further discussed in Section 4.1.

3.2. Spatial Coverage of Main Algorithm

As a key indicator of the quality of retrievals, the algorithm path of each pixel is stored in the LAI/FPAR products. By comparing the retrieval rate of different algorithm paths at global scale, we can evaluate the overall quality of the products from C5 and C6. The main algorithm outputs retrievals at high precision in the case of low LAI and at moderate precision when LAI is high and surface reflectance has low sensitivity to LAI. In the case of main algorithm failure, low-precision retrievals are obtained from the empirical back-up algorithm. Figure 3a compares the biome-specific yearly and globally averaged retrieval rate of different algorithm paths. C6 and C5 show similar patterns for all biomes except biome 5 (evergreen broadleaf forests) and biome 7 (evergreen needleleaf forest). C6 shows 17% and 7% higher main algorithm retrieval rates than C5 for biomes 5 and 7, respectively. This improvement is due to an updated biome map, which will be discussed in Section 4.1. As the main algorithm has better performance than the backup algorithm, the success rate of the main algorithm (Retrieval Index, RI) can be seen as a quality indicator. The RI of all biome types except biomes 5 and 7 is higher than 90%. Biomes 1 to 4 have the highest RI (more than 95%). The retrieval rate of main algorithm without saturation is lowest in the case of evergreen broadleaf forests because of reflectance saturation in dense canopies. This means the reflectances do not contain sufficient information to localize a LAI value. The other three forest types also show a large proportion of retrievals under saturation. Because evergreen needleleaf forests are located in the high latitude regions where the solar zenith angles are low in winter season, biome 7 shows obvious backup algorithm retrievals that are due to poor sun-sensor geometry. Nevertheless, C6 shows slightly higher RI than C5.

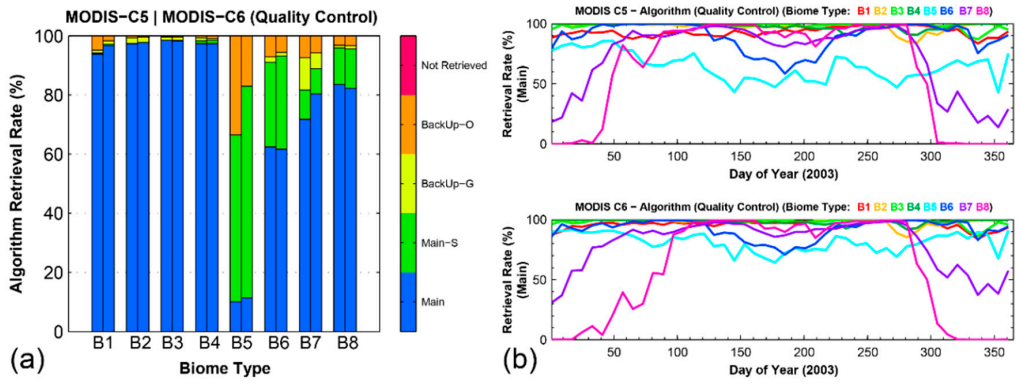

Figure 3. Comparison of global retrieval rate of different algorithm paths (retrieval index) for eight biome types. (**a**) Yearly and globally averaged (in 2003) retrieval rate of different algorithm paths. Possible algorithm paths are (i) Main (Main algorithm without saturation); (ii) Main-S (Main algorithm with saturation); (iii) BackUp-G (Backup algorithm because of bad sun-sensor geometry); (iv) BackUp-O (Backup algorithm because of other reasons) and (v) Not Retrieved (not executed because BRF data are not available). For each biome, the left bar is for C5 and right one is for C6; (**b**) Annual variation of main algorithm spatial coverage in 2003 (upper plot is for C5 and lower plot is for C6). This statistic is done after quality control using cloud and aerosol flags.

The seasonal variations of RI in C5 and C6 for all eight biomes in 2003 shown in Figure 3b indicate that the annual cycles of C6 and C5 are quite consistent. As in Figure 3a, the RI of biome 5 has been improved from C5 to C6. A strong seasonality is seen in needleleaf forests (biomes 7 and 8) with RI varying from about 90% during the boreal summer to less than 30% during the boreal winter. The RI of deciduous needleleaf forests can even be zero in the boreal winter season. The decrease of RI in the boreal winter results from unsuitable illumination conditions, extreme solar zenith angles, and snow or cloud contamination. The fact that almost all needleleaf forests appear only in the northern hemisphere makes the seasonal variation more obvious.

3.3. Seasonal LAI/FPAR Variations

Seasonal variations in C5 and C6 LAI/FPAR retrievals are shown in Figure 4 and Figure S3. These lines show globally averaged biome-specific LAI/FPAR values as a function of Julian day in 2003. This analysis only uses retrievals derived by the main algorithm. We note that C5 and C6 products show good consistency of LAI/FPAR seasonal variations. All biome types except for evergreen broadleaf forests and savannas show seasonality at different levels. The retrievals over deciduous forests demonstrate expected obvious seasonality in both LAI and FPAR. LAI of deciduous broadleaf forests (deciduous needleleaf forests) drops from around 5 (3) in boreal summer to around 0.5 (<0.5) in boreal winter. With ample illumination in tropics and subtropics, evergreen broadleaf forests have LAI values of about 5 through the year with negligible seasonal variations. By checking the seasonal variations of the algorithm path (see Figure S4), we find that the missing part in case of deciduous needleleaf forests is due to unavailable retrievals from main algorithm because of bad sun-sensor geometry (solar zenith angle larger than 52.5° or view zenith angle larger than 67.5°). Seasonal variations of algorithm path can also explain these erratic artifacts in LAI/FPAR variations (e.g., the sudden drop at DOY 10 to 20 and the peak around DOY 200 for deciduous needleleaf forests in Figure 4a).

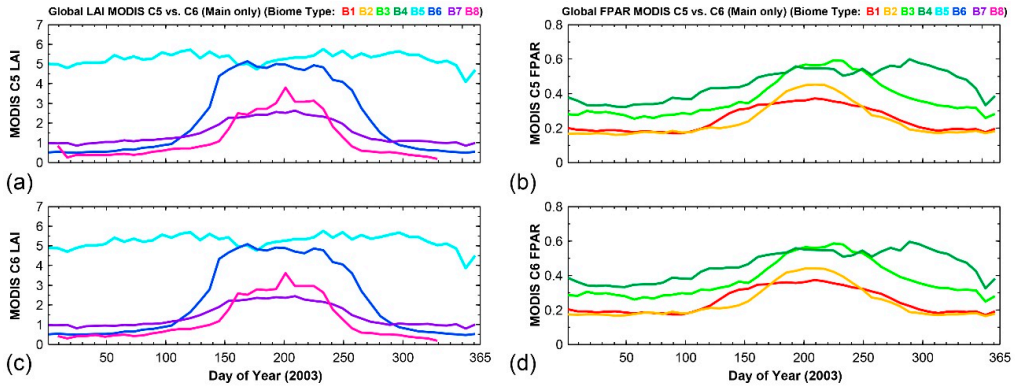

Figure 4. Seasonal variations of globally averaged MODIS (**a**) LAI C5; (**b**) FPAR C5; (**c**) LAI C6; and (**d**) FPAR C6 in 2003. Left panels show seasonal LAI trajectories over four different forest types (evergreen broadleaf forest (B5), deciduous broadleaf forest (B6), evergreen needle leaf forest (B7) and deciduous needle leaf forest (B8)). FPAR panels (right) show other four non-forest biome types (grasses/cereal crops (B1), shrubs (B2), broadleaf crops (B3) and savannas (B4)). LAI of non-forest biome types and FPAR of forest types are shown in Figure S3 for the sake of clarity.

3.4. Inter-Annual LAI Anomalies

In this section, we check the consistency of 13 years (2002–2014) of LAI anomalies from C5 and C6. The importance of this work is two-fold. First, an LAI anomaly represents the difference between LAI values of a specific year and the multi-year mean LAI value, from which we can deduce potential annual variations in carbon, water and energy balances. Second, using independent geographic variables to explain the annual variation of LAI is a good way to validate the products indirectly.

The spatial and temporal averages of LAI anomalies from C5 and C6 during the period from 2002 to 2014 (2000 and 2001 were discarded because of missing data) are compared in Figure 5. Panel (a) shows the anomaly of annual averaged LAI in two precipitation-limited regions (Eastern Australia and Northeastern Brazil). For both regions, C5 and C6 LAI anomalies match very well. The correlation coefficients between C5 and C6 in the two regions are 0.972 and 0.975, respectively. The LAI in Northeastern Brazil shows a large decrease in 2012, which can be explained by the severe drought in Northeast Brazil in that year [27]. Panel (b) shows anomaly of growing season (May to September) averaged LAI in two temperature-limited regions (North America and Eurasia). Also for these two regions, C5 and C6 show similar LAI annual variations. We note that the slopes of C6 are slightly higher than C5 in all these plots. This is because the improved sensor calibration of C6 solved the Terra MODIS sensor degradation issue in C5 [28]. A more detailed explanation for these LAI inter-annual variations will be presented in the second part of this two-paper series.

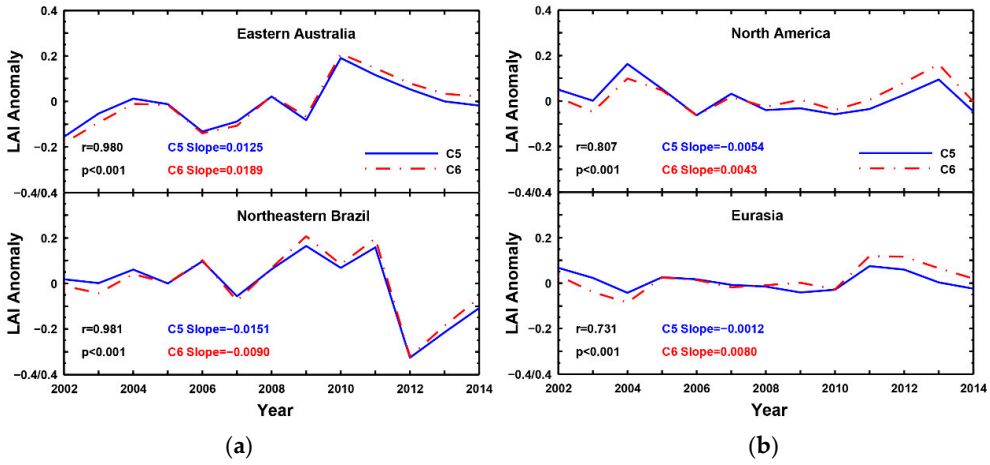

Figure 5. Comparison of anomalies of spatially averaged LAI values from C5 (blue solid lines) and C6 (red dashed lines). Panel (**a**) shows the anomaly of annual averaged LAI in two precipitation-limited regions (Eastern Australia, 20°S–40°S, 145°E–155°E and Northeastern Brazil, 3°S–12°S, 35°W–45°W). Panel (**b**) shows the anomaly of growing season (May to September) averaged LAI in two temperature-limited high latitude (>60°N) regions (North America and Eurasia). Correlation coefficient (r) between the two MODIS collections and its significance (p) are given in each panel. Moreover, slopes are provided as indicators of the trend of inter-annual LAI.

4. Benefits from Improved Input Data

From the above comparisons, we see there are no significant discrepancies between C5 and C6 products in terms of global distribution, seasonal variations, inter-annual LAI anomalies and spatial coverage of high quality retrievals. However, pixel-to-pixel comparison still shows differences between C5 and C6 at the regional scale. As C6 inherits the algorithm and LUTs from C5 directly, the improvements in input data and change of spatial resolution are the only two sources of LAI/FPAR differences between the two versions. Here we investigate and quantify the impact of input changes and the scale effect of the algorithm.

4.1. Benefits from Biome Map Improvement

As an important prior knowledge about the land surface, a biome map is utilized to reduce the number of unknowns in the inverse problem of LAI/FPAR estimation. In the operational algorithm, structurally and spectrally different parameterization in 3D RT is used for each biome type. Specification of biome type for each pixel is thus critically important to choose the correct RT dependent LUT for LAI/FPAR estimation. Errors in biome classification can therefore propagate into LAI/FPAR retrievals. Numerical experiments suggest that a mismatch in biome specific LUT will result in either

a low RI and/or incorrect LAI/FPAR values [1]. Conversely, increased biome accuracy will help to reduce uncertainty in LAI/FPAR products. As LAI/FPAR production requires prior knowledge of surface biome type, the biome input is generally based on an earlier version of land-cover product. This means C4 and C5 land-cover products have been used for C5 and C6 LAI/FPAR production, respectively. Biome input (based on C5 MODIS land-cover product) for C6 LAI/FPAR production is reported to be substantially improved relative to the biome input (based on C4 MODIS land-cover product) for C5 LAI/FPAR production in terms of accuracy, stability across years due to refinements in the land-cover classification algorithm and ancillary datasets used [24].

Figure 6a shows the proportion of pixels derived from each biome type in the C6 biome map for each class in the C5 biome type at the global scale during 2001 to 2003. Some biomes in C6, for example biomes 1, 2, 4, 5 and 8, are relatively consistent with C5 (more than 70% consistency). Around 30% of the pixels labeled as biome 6 and biome 7 in C5 change to other biome types in C6. Compared to other biomes, biome 3 has the largest proportion of differently classified biome cases. Around 50% of biome 3 pixels in C5 are classified into biome 1 in C6. We note that most of the differently classified pixels change to their neighboring biome types, which have similar canopy structural characteristics in RT realization. For instance, most of the "changed" pixels in biome 3 (broadleaf crops) are labeled as biome 1 (grass and cereal crop) in C6. This result agrees with [24].

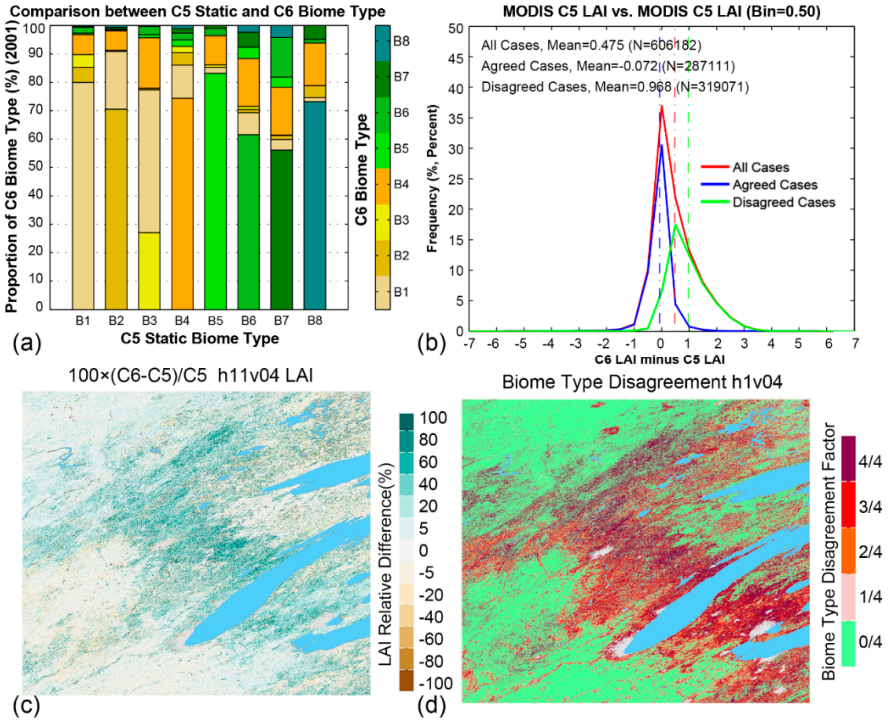

Figure 6. Impact of input biome map change on LAI/FPAR retrievals. (**a**) Areal proportion of globally changed biome type from static C5 to dynamic C6 input biome type (2001–2003). Proportions of C6 biomes are calculated with respect to total area in each C5 biome type; (**b**) Histogram of the difference between C5 and C6 LAI values in tile h11v04 (red box in Figure 7) during 12th–19th July of 2003. The blue line and green line show consistent biome type and changing biome type, respectively; (**c**) Spatial distribution of relative difference in LAI between C5 and C6 in tile h11v04 (dominant biome type is broadleaf crops); (**d**) Spatial distribution of BTDF (biome type disagreement factor) showing how many 500 m C6 pixels in a 1 km C5 pixel are different with the C5 biome type.

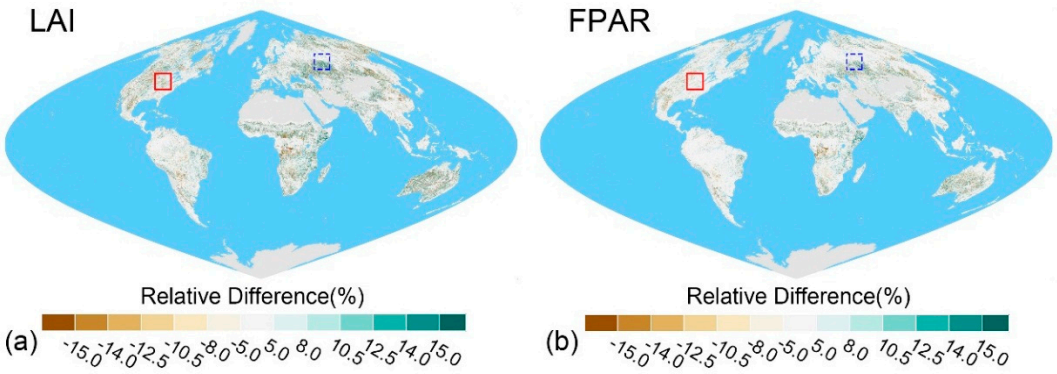

Figure 7. Spatial distribution of relative difference (100 × (C6-C5)/C5) for pixels with the same biome types (BTDF = 0) during 12th July to 19th July in 2003. (**a**) LAI; (**b**) FPAR. Detailed results from two tiles (h11v04 and h22v03) shown as red and blue boxes are given in Figure 8.

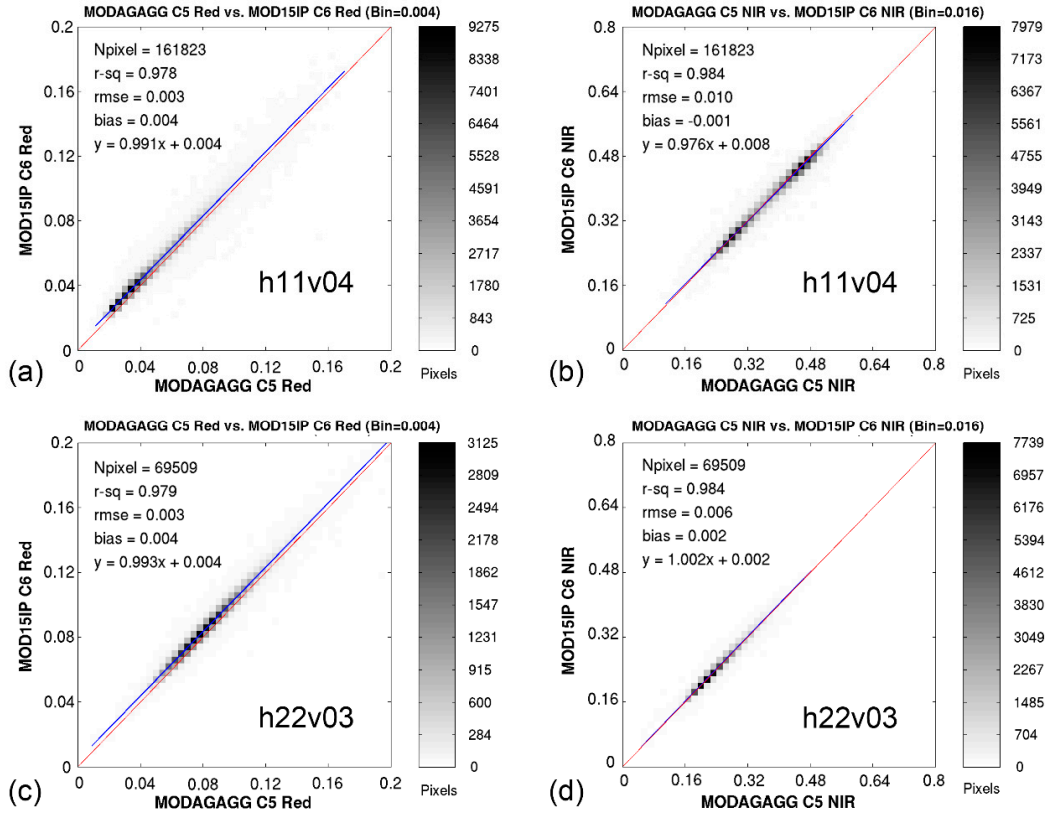

Figure 8. Density scatter plots of land surface reflectance (BRFs) of red band (left panels) and NIR band (right panels) of the two example tiles (**a**) and (**b**) are for tile h11v04; (**c**) and (**d**) are for h22v03 shown as boxes in Figure 7.

To quantify the impact of biome type change on LAI retrievals, we investigate the tile (1200 by 1200 km) h11v04 as an example as 53% of this region shows changes between C5 and C6. We divide all pixels into two categories, pixels with consistent and changed biome types, and compare the LAI differences. Histograms of the difference for these two categories and for all pixels are shown in Figure 6b. The mean difference of all pixels with consistent biome type (about 27% of pixels) is −0.072, which is obviously smaller than that of all pixels with changing biome types (0.968). The mean difference of all pixels in this tile is 0.475. Such biased patterns are depicted in Figure 6c,d.

For further investigation, we define the biome type disagreement factor (BTDF) as the proportion of pixels with changing biome type. As four 500 m C6 pixels compose a 1 km C5 biome type, this factor can be 0, 1/4, 1/2, 3/4 or 1. It can be seen that when there is no biome type change, the relative difference in LAI will be within ±5%. This can be as high as ±100% in pixels with changing biome type. In particular, note that the directionality of observed difference is not uniform across cases of biome change.

The mean value and standard deviation of the difference and RMSE between C5 and C6 LAI are listed in Table 1 (Table S1 shows the same for FPAR). When the biome type disagreement factor is small (0/4 or 1/4), C6 retrievals underestimate C5 for most biome type cases. Interestingly, the discrepancy between C5 and C6 gets larger with increasing biome type disagreement factor. With the same biome input (BTDF = 0/4), the mean RMSE of LAI and FPAR are 0.29 and 0.091, respectively, but biome type disagreement worsened the consistency (LAI: 0.39, FPAR: 0.102). Overall C6 estimates global LAI and FPAR by C5-0.01 and C5-0.004, respectively.

Table 1. Biome specific differences between C5 and C6 LAI at the global scale in 2003. Mean value and standard deviation of the difference and RMSE (values in brackets) between C5 and C6 (C6 minus C5) are listed in the table.

Biome Type	BTDF = 0/4	BTDF = 1/4	BTDF = 2/4	BTDF = 3/4	BTDF = 4/4
Grasses/Cereal crops (B1)	0.00 ± 0.24 (0.24)	−0.01 ± 0.30 (0.30)	0.01 ± 0.33 (0.33)	0.02 ± 0.39 (0.39)	0.08 ± 0.43 (0.44)
Shrubs (B2)	−0.01 ± 0.15 (0.15)	0.02 ± 0.21 (0.21)	0.04 ± 0.24 (0.24)	0.06 ± 0.25 (0.25)	0.05 ± 0.23 (0.24)
Broadleaf crops (B3)	−0.02 ± 0.22 (0.22)	0.11 ± 0.23 (0.25)	0.21 ± 0.28 (0.35)	0.31 ± 0.35 (0.46)	0.42 ± 0.40 (0.57)
Savanna (B4)	0.00 ± 0.26 (0.26)	−0.04 ± 0.30 (0.30)	−0.07 ± 0.36 (0.37)	−0.11 ± 0.42 (0.43)	−0.16 ± 0.40 (0.43)
[1] EBF (B5)	−0.08 ± 0.62 (0.63)	−0.45 ± 0.65 (0.79)	−0.88 ± 0.71 (1.12)	−1.32 ± 0.82 (1.55)	−1.71 ± 1.00 (1.98)
[2] DBF (B6)	−0.09 ± 0.48 (0.49)	−0.01 ± 0.48 (0.48)	0.05 ± 0.52 (0.52)	0.10 ± 0.58 (0.58)	0.03 ± 0.52 (0.52)
[3] ENF (B7)	−0.17 ± 0.51 (0.54)	−0.23 ± 0.50 (0.55)	−0.31 ± 0.54 (0.62)	−0.40 ± 0.60 (0.72)	−0.45 ± 0.73 (0.85)
[4] DNF (B8)	−0.19 ± 0.57 (0.60)	−0.26 ± 0.56 (0.62)	−0.38 ± 0.61 (0.72)	−0.49 ± 0.68 (0.84)	−0.58 ± 0.82 (1.00)
Mean	−0.02 ± 0.29 (0.29)	−0.03 ± 0.33 (0.33)	−0.02 ± 0.40 (0.40)	−0.02 ± 0.50 (0.50)	0.02 ± 0.60 (0.60)
Overall			−0.01 ± 0.39 (0.39)		

[1] Evergreen broadleaf forest; [2] Deciduous broadleaf forest; [3] Evergreen needleleaf forest; [4] Deciduous needleleaf forest.

4.2. Benefits from Surface Reflectance Improvement

To elucidate the impact of changes in input surface reflectance, we only focus on pixels with consistent biome type (BTDF = 0). Between Table 1 and Table S1, we can see that C6 LAI and FPAR values of all biomes, except biomes 1 and 4 for LAI and biome 4 for FPAR, are smaller than C5. Figure 7a,b shows the global distribution of relative difference (100 × (C6-C5)/C5) of LAI and FPAR. h11v04 (red box) and h22v03 (blue box) are two example tiles showing lower and higher C6 LAI estimation cases, respectively. As expected, both LAI and FPAR display similar spatial patterns. By only considering biome input consistent pixels, differences in LAI and FPAR between C5 and C6 vary within ±15%. Possible explanations for this discrepancy are two-fold: surface reflectance input changes and scale effect of the algorithm, further discussed below.

Comparisons of reflectance between C5 and C6 are shown in Figure 8. Panels (a) and (b) are for tile h11v04 (Figure 7) in which C6 underestimates C5. Panels (c) and (d) are for tile h22v03 (Figure 7) in which C6 overestimates C5. In both tiles, NIR (near-infrared) band reflectance shows good consistency between the two versions. However, the red band reflectances in C6 are relatively higher than in C5, especially at the lower range of reflectances. As leaves in the canopy absorb more red photons,

higher red reflectances will lead to lower LAI retrievals. These changes in reflectances resulted from refinements to the atmospheric correction algorithm. The overestimation in C6 over the tile h22v03 could be explained by the scale effects which are discussed below.

4.3. Impact of Scale Effect

With the development of quantitative remote sensing, scale effects, as a common phenomenon, have attracted more and more attention from the community. The term "scale" is widely used in many other fields as with as remote sensing and has different meanings in various disciplines [29]. In this paper, scale effects refer to the discrepancy between two products derived from the same algorithm but at different spatial resolutions. As mentioned above, MODIS LAI/FPAR products improved the spatial resolution from 1 km to 500 m using the same retrieval algorithm, which raises two questions: (1) what is the behavior of the scale effect in LAI/FPAR product and algorithm and (2) is the difference caused by the scale effect negligible? Figure 9 theoretically demonstrates the relationship between the two LAI products (C5 and C6). The discrepancy between LAI1 and LAI2 is caused by both heterogeneity of land surface and nonlinear characteristics of the retrieval models [29]. On the one hand, landscape homogeneity cannot be assumed especially in the case of a coarser spatial resolution footprint. In other words, a MODIS pixel should be considered as a mosaic of different biome types. On the other hand, the radiative transfer-based algorithm is scale-dependent [1]. This is because the pixels are likely to contain an increasing amount of radiative contribution from the background [30]. Thus, the MODIS LAI/FPAR products are scale-dependent and the scale effect could be one of the causal factors introducing a certain level of discrepancy between C5 and C6.

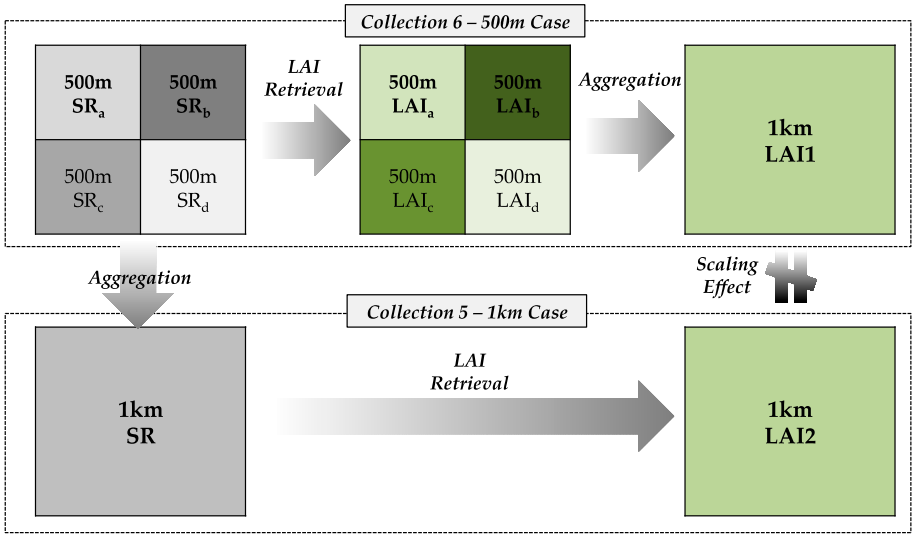

Figure 9. Theoretical description of scale effect.

To understand the discrepancy between C5 and C6 products due to scale effects, we conducted a simulation experiment using biome 6 (deciduous broadleaf forests) as an example. Note that the simulation results will not be similar across biome types due to biome-specific RT parameterizations. Only retrievals from the main RT based algorithm were analyzed. We simulated the heterogeneity in one 1 km (C5) pixel by adding 5% or 15% bias on NIR reflectance (red reflectance is fixed) for four 500 m (C6) pixels. Figure 10 shows the results of this experiment. The LAI values for C5 were selected along the black line in the red-NIR spectral space depicted in Figure 10a. It is clear that the relationship between LAI and reflectance is nonlinear. Moreover, there is a clear division between the saturated and unsaturated parts. This is more obvious in Figure 10b where both LAI and FPAR show an inflection point when saturation appears. Irrespective of saturation, the relationship between LAI and NIR reflectance is roughly a concave function. In this relationship, if reflectance SR2 is the

mean value of SR1 and SR3, the LAI (SR2) is smaller than the mean value of LAI (SR1) and LAI (SR3). Before saturation, the relationship between FPAR and NIR reflectance is almost linear. When saturation appears, the relationship changes to a concave function as well. The short parallel lines at small LAI and FPAR indicate that LAI or FPAR does not vary with NIR reflectance. This is because of sparse distribution of retrievals in the LUT at low LAI values [31].

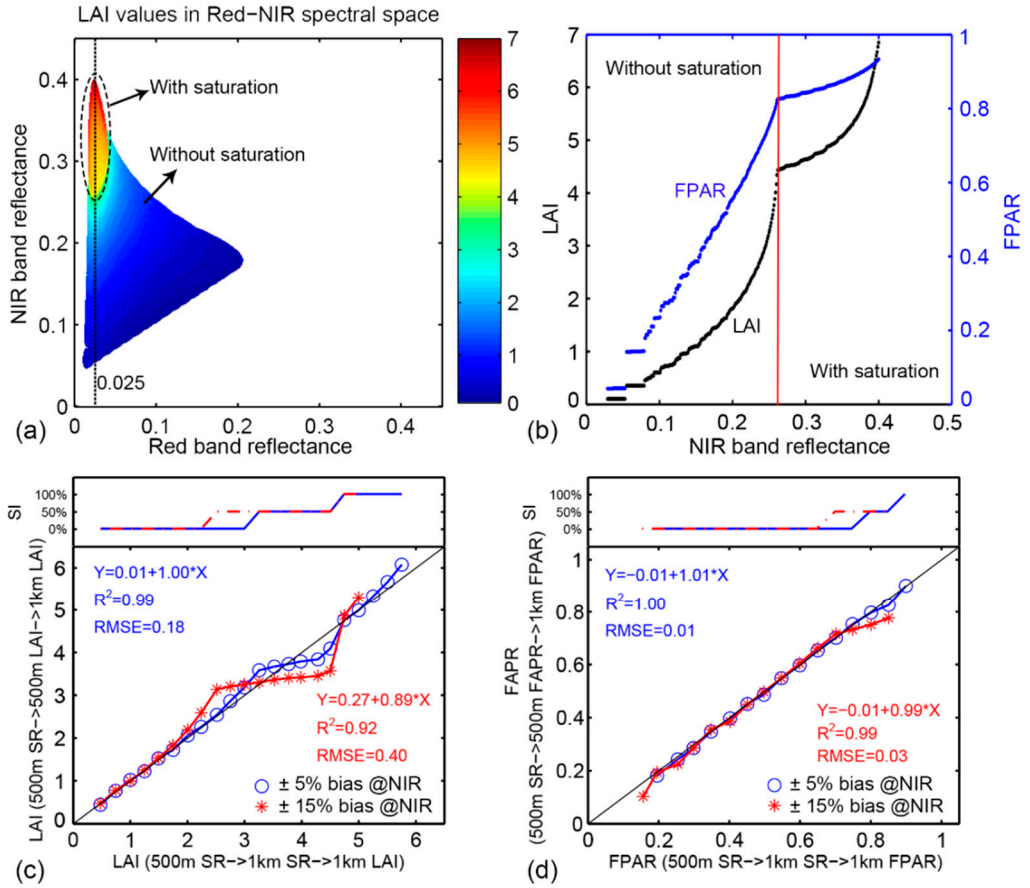

Figure 10. Scale effect of MODIS LAI/FPAR main algorithm. Biome 6 (deciduous broadleaf forests) is used as an example here. The solar zenith angle is fixed at 30° and the view direction is nadir. (**a**) Distribution of LAI values derived from the main RT based algorithm in the Red-NIR spectral space. Equally spaced LAI values along the vertical black line (red = 0.025) are selected as experimental retrievals from C5 (LAIc5). The corresponding reflectances of C5 are REDc5 and NIRc5. Let the red reflectance of all the four C6 pixels (REDc6) be equal to REDc5. To satisfy the energy conservation law, we add a positive bias to NIRc5 to obtain NIRc6_1 for two C6 pixels and add a negative bias to NIRc5 to obtain NIRc6_2 for the two left C6 pixels. Thus, four C6 LAIs can be derived using REDc6 and NIRc6; (**b**) Denotes the variations of LAI (black points) and FPAR (blue points) with NIR reflectance along the black line in (**a**). Retrievals with and without saturation are separated by a red line; (**c**,**d**) demonstrate the discrepancy in LAI and FPAR caused by scale effects, respectively. 5% and 15% bias are shown in blue and red. The saturation index (SI) for different LAI (FPAR) values is also plotted in the figures.

The discrepancy in LAI and FPAR due to scale effects is demonstrated in Figure 10c,d. The x-axis and y-axis can be seen as C5 products and C6 products, respectively. The four retrievals of C6 pixels can be partially and completely derived from unsaturated or saturated algorithmic conditions because of the bias in NIR reflectance. We define the Saturation Index (SI) as the proportion of unsaturated pixels. When SI equals 0% (all retrievals from the unsaturated part), there is no obvious difference between C5 and C6 LAI values at a low range of LAI values. However, C6 LAI tends to be higher than C5 with an increase in LAI. When SI is about 50% (two retrievals from unsaturated and the other

two from saturated part), C6 LAI tends to be smaller than C5. When SI equals 100%, C6 LAI increases again. These changes can be explained by the relationship between LAI and NIR reflectance shown in Figure 10b. As expected, a 15% bias causes a larger scale effect than a 5% bias (RMSE 0.4 *vs.* 0.18). Compared to LAI, FPAR shows less and even negligible scale effects with RMSE 0.01 and 0.03 for 5% and 15% bias. This is because the FPAR-reflectance relationship is almost linear, especially prior to saturation conditions. Because of the regional convex relationship when saturation starts to appear, C6 can be lower than C5.

5. Conclusions

This paper presents version consistency and improvements in the latest MODIS LAI/FPAR C6 product. Compared to previous C5, the most important change in C6 is that the products are being produced at 500 m spatial resolution instead of 1 km. In addition, as discussed here, C6 benefited from improved surface reflectances and biome type inputs. The refined C6 atmospheric correction algorithm generates relatively higher red band reflectances, which results in lower LAI/FPAR values. The new multi-year land-cover product provides biome type input to the algorithm with better accuracy. The differences caused by scale effects are found to be negligible for FPAR and in cases where LAI is low. Scale effects can explain some of the discrepancy between 1 km C5 and 500 m C6 products, especially for cases of high LAI values. In view of these changes in inputs and spatial resolution, a consistency check of C6 products with C5 was performed in terms of global distributions, spatial coverage of high quality retrievals, seasonal variations and inter-annual LAI anomalies. From these analyses, we found no significant discrepancies between C5 and C6 LAI/FPAR products. The proportion of main radiative transfer algorithm retrievals in C6 increases slightly in most biome types, notably including 17% improvement in evergreen broadleaf forests. With the same biome input, the mean RMSEs of LAI and FPAR are 0.29 and 0.091, respectively, but biome type disagreement worsens the consistency (LAI: 0.39, FPAR: 0.102). Overall C6 estimates global LAI and FPAR by C5-0.01 and C5-0.004. Moreover, C5 and C6 shows consistent inter-annual LAI anomalies over two temperature-limited regions and two precipitation-limited regions. These results produce confidence in the new C6 products. Further evaluation of MODIS LAI/FPAR C6 products through validation using field measurements and inter-comparison with other exiting products will be presented in the second part of this series.

Supplementary Materials: The following are available online at www.mdpi.com/2072-4292/8/5/359, Figure S1: Three-year global 500 m eight-biome map used for MODIS LAI/FPAR C6 products from 2001 to 2003; Figure S2: Color-coded maps of MODIS C5 and C6 FPAR for January (17th–24th January) and July (12th–19th July) of 2003; Figure S3: Seasonal variations of globally averaged MODIS LAI and FPAR from C5 and C6 in 2003; Figure S4: Seasonal variations of algorithm path of C5 and C6 in 2003; Table S1: Biome type specific differences between C5 and C6 FPAR for global scale in 2003.

Acknowledgments: Help from MODIS & VIIRS Science team members is gratefully acknowledged. This work is supported by the MODIS program of NASA and partially funded by the National Basic Research Program of China (Grant No. 2013CB733402), the key program of NSFC (Grant No. 41331171) and Chinese Scholarship Council.

Author Contributions: Kai Yan, Yuri Knyazikhin, Ramakrishna R. Nemani and Ranga B. Myneni conceived and designed the experiments; Taejin Park and Kai Yan performed the experiments; Chi Chen, Taejin Park and Bin Yang analyzed the data; Zhao Liu and Guangjian Yan contributed to Sections 3.4 and 4.3 respectively. All authors contributed to the writing of the paper.

Conflicts of Interest: The authors declare no conflict of interest.

Abbreviations

The following abbreviations are used in this manuscript:

MODIS	Moderate Resolution Imaging Spectroradiometer
LAI	Leaf Area Index
FPAR	Fraction of Photosynthetically Active Radiation

C3	Collection 3
C4	Collection 4
C5	Collection 5
C6	Collection 6
RT	Radiative Transfer
LUT	Look-Up-Table
BRF	Bi-directional Reflectance Factors
NDVI	Normalized Difference Vegetation Index
QC	Quality Control
BTDF	Biome Type Disagreement Factor
RI	Retrieval Index
SI	Saturation Index

References

1. Myneni, R.B.; Smith, G.R.; Lotsch, A.; Friedl, M.; Morisette, J.T.; Votava, P.; Running, S.W.; Hoffman, S.; Knyazikhin, Y.; Privette, J.L.; *et al.* Global products of vegetation leaf area and fraction absorbed PAR from year one of MODIS data. *Remote Sens. Environ.* **2002**, *83*, 214–231. [CrossRef]
2. Sellers, P.J.; Dickinson, R.E.; Randall, D.A.; Betts, A.K.; Hall, F.G.; Berry, J.A.; Collatz, G.J.; Denning, A.S.; Mooney, H.A.; Nobre, C.A. Modeling the exchanges of energy, water, and carbon between continents and the atmosphere. *Science* **1997**, *275*, 502–509. [CrossRef] [PubMed]
3. Zhu, Z.; Bi, J.; Pan, Y.; Ganguly, S.; Anav, A.; Xu, L.; Samanta, A.; Piao, S.; Nemani, R.; Myneni, R. Global data sets of vegetation leaf area index (LAI)3g and Fraction of Photosynthetically Active Radiation (FPAR)3g derived from Global Inventory Modeling and Mapping Studies (GIMMS) Normalized Difference Vegetation Index (NDVI3g) for the Period 1981 to 2011. *Remote Sens.* **2013**, *5*, 927–948.
4. Knyazikhin, Y.; Martonchik, J.V.; Myneni, R.B.; Diner, D.J.; Running, S.W. Synergistic algorithm for estimating vegetation canopy leaf area index and fraction of absorbed photosynthetically active radiation from MODIS and MISR data. *J. Geophys. Res. Atmos.* **1998**, *103*, 32257–32275. [CrossRef]
5. Knyazikhin, Y.; Glassy, J.; Privette, J.L.; Tian, Y.; Lotsch, A.; Zhang, Y.; Wang, Y.; Morisette, J.T.; Votava, P.; Myneni, R.B. *MODIS Leaf Area Index (LAI) and Fraction of Photosynthetically Active Radiation Absorbed by Vegetation (FPAR) Product (MOD15) Algorithm Theoretical Basis Document*; Theoretical Basis Document; NASA Goddard Space Flight Center: Greenbelt, MD, USA, 1999; pp. 1–170.
6. Yang, W.; Tan, B.; Huang, D.; Rautiainen, M.; Shabanov, N.V.; Wang, Y.; Privette, J.L.; Huemmrich, K.F.; Fensholt, R.; Sandholt, I.; *et al.* MODIS leaf area index products: From validation to algorithm improvement. *IEEE Trans. Geosci. Remote Sens.* **2006**, *44*, 1885–1898. [CrossRef]
7. Yang, W.; Huang, D.; Tan, B.; Stroeve, J.C.; Shabanov, N.V.; Knyazikhin, Y.; Nemani, R.R.; Myneni, R.B. Analysis of leaf area index and fraction of PAR absorbed by vegetation products from the terra MODIS sensor: 2000–2005. *IEEE Trans. Geosci. Remote Sens.* **2006**, *44*, 1829–1842. [CrossRef]
8. Yang, W.; Shabanov, N.V.; Huang, D.; Wang, W.; Dickinson, R.E.; Nemani, R.R.; Knyazikhin, Y.; Myneni, R.B. Analysis of leaf area index products from combination of MODIS Terra and Aqua data. *Remote Sens. Environ.* **2006**, *104*, 297–312. [CrossRef]
9. Shabanov, N.V.; Knyazikhin, Y.; Baret, F.; Myneni, R.B. Stochastic Modeling of Radiation Regime in Discontinuous Vegetation Canopies. *Remote Sens. Environ.* **2000**, *74*, 125–144. [CrossRef]
10. Buermann, W. Analysis of a multiyear global vegetation leaf area index data set. *J. Geophys. Res.* **2002**, *107*, D22. [CrossRef]
11. Ganguly, S.; Samanta, A.; Schull, M.A.; Shabanov, N.V.; Milesi, C.; Nemani, R.R.; Knyazikhin, Y.; Myneni, R.B. Generating vegetation leaf area index Earth system data record from multiple sensors. Part 2: Implementation, analysis and validation. *Remote Sens. Environ.* **2008**, *112*, 4318–4332. [CrossRef]
12. Fang, H.; Jiang, C.; Li, W.; Wei, S.; Baret, F.; Chen, J.M.; Garcia-Haro, J.; Liang, S.; Liu, R.; Myneni, R.B.; *et al.* Characterization and intercomparison of global moderate resolution leaf area index (LAI) products: Analysis of climatologies and theoretical uncertainties. *J. Geophys. Res. Biogeosci.* **2013**, *118*, 529–548. [CrossRef]
13. Majasalmi, T.; Rautiainen, M.; Stenberg, P.; Manninen, T. Validation of MODIS and GEOV1 fPAR Products in a Boreal Forest Site in Finland. *Remote Sens.* **2015**, *7*, 1359–1379. [CrossRef]

14. Garrigues, S.; Lacaze, R.; Baret, F.; Morisette, J.T.; Weiss, M.; Nickeson, J.E.; Fernandes, R.; Plummer, S.; Shabanov, N.V.; Myneni, R.B.; *et al.* Validation and intercomparison of global Leaf Area Index products derived from remote sensing data. *J. Geophys. Res.* **2008**, *113*. [CrossRef]
15. Ross, J. *The Radiation Regime and Architecture of Plants Stands*; Springer Science & Business Media: Medford, MA, USA, 1981.
16. Myneni, R.B.; Ross, J. *Photon-Vegetation Interactions: Applications in Optical Remote Sensing and Plant Ecology*; Springer Science & Business Media: Medford, MA, USA, 1991.
17. Huang, D.; Knyazikhin, Y.; Dickinson, R.E.; Rautiainen, M.; Stenberg, P.; Disney, M.; Lewis, P.; Cescatti, A.; Tian, Y.; Verhoef, W.; *et al.* Canopy spectral invariants for remote sensing and model applications. *Remote Sens. Environ.* **2007**, *106*, 106–122. [CrossRef]
18. Myneni, R.B.; Williams, D.L. On the relationship between FAPAR and NDVI. *Remote Sens. Environ.* **1994**, *49*, 200–211. [CrossRef]
19. Wang, Y.; Tian, Y.; Zhang, Y.; El-Saleous, N.; Knyazikhin, Y.; Vermote, E.; Myneni, R.B. Investigation of product accuracy as a function of input and model uncertainties: Case study with SeaWiFS and MODIS LAI/FPAR algorithm. *Remote Sens. Environ.* **2001**, *78*, 299–313. [CrossRef]
20. Myneni, R.B.; Ramakrishna, R.; Nemani, R.; Running, S.W. Estimation of global leaf area index and absorbed par using radiative transfer models. *IEEE Trans. Geosci. Remote Sens.* **1997**, *35*, 1380–1393. [CrossRef]
21. Fang, H.; Li, W.; Myneni, R.B. The impact of potential land cover misclassification on MODIS leaf area index (LAI) estimation: A statistical perspective. *Remote Sens.* **2013**, *5*, 830–844. [CrossRef]
22. Garrigues, S.; Shabanov, N.V.; Swanson, K.; Morisette, J.T.; Baret, F.; Myneni, R.B. Intercomparison and sensitivity analysis of Leaf Area Index retrievals from LAI-2000, AccuPAR, and digital hemispherical photography over croplands. *Agric. Forest Meteorol.* **2008**, *148*, 1193–1209. [CrossRef]
23. Vermote, E.F.; Vermeulen, A. Atmospheric Correction Algorithm: Spectral Reflectances (MOD09). Algorithm Theoretical Background Document. Available online: http://dratmos.geog.umd.edu/files/pdf/atbd_mod09.pdf (accessed on 7 March 2016).
24. Friedl, M.A.; Sulla-Menashe, D.; Tan, B.; Schneider, A.; Ramankutty, N.; Sibley, A.; Huang, X. MODIS Collection 5 global land cover: Algorithm refinements and characterization of new datasets. *Remote Sens. Environ.* **2010**, *114*, 168–182. [CrossRef]
25. Wolfe, R.E.; Devadiga, S.; Masuoka, E.J.; Running, S.W.; Vermote, E.; Giglio, L.; Wan, Z.; Riggs, G.A.; Schaaf, C.; Myneni, R.B.; *et al.* Improvements to the MODIS Land Products in Collection Version 6. Available online: http://adsabs.harvard.edu/abs/2013AGUFM.B41D0430W (accessed on 7 March 2016).
26. Masson, V.; Champeaux, J.; Chauvin, F.; Meriguet, C.; Lacaze, R. A global database of land surface parameters at 1-km resolution in meteorological and climate models. *J. Climat.* **2003**, *16*, 1261–1282. [CrossRef]
27. Marengo, J.A.; Alves, L.M.; Soares, W.R.; Rodriguez, D.A.; Camargo, H.; Riveros, M.P.; Pabló, A.D. Two contrasting severe seasonal extremes in tropical South America in 2012: Flood in Amazonia and drought in northeast Brazil. *J. Climat.* **2013**, *26*, 9137–9154. [CrossRef]
28. Wang, D.; Morton, D.; Masek, J.; Wu, A.; Nagol, J.; Xiong, X.; Levy, R.; Vermote, E.; Wolfe, R. Impact of sensor degradation on the MODIS NDVI time series. *Remote Sens. Environ.* **2012**, *119*, 55–61. [CrossRef]
29. Wu, H.; Li, Z. Scale Issues in Remote Sensing: A Review on Analysis, Processing and Modeling. *Sensors* **2009**, *9*, 1768–1793. [CrossRef] [PubMed]
30. Tian, Y.; Wang, Y.; Zhang, Y.; Knyazikhin, Y.; Bogaert, J.; Myneni, R.B. Radiative transfer based scaling of LAI retrievals from reflectance data of different resolutions. *Remote Sens. Environ.* **2003**, *84*, 143–159. [CrossRef]
31. Ganguly, S.; Schull, M.A.; Samanta, A.; Shabanov, N.V.; Milesi, C.; Nemani, R.R.; Knyazikhin, Y.; Myneni, R.B. Generating vegetation leaf area index earth system data record from multiple sensors. Part 1: Theory. *Remote Sens. Environ.* **2008**, *112*, 4333–4343. [CrossRef]

remote sensing

MDPI

Article

Evaluation of MODIS LAI/FPAR Product Collection 6. Part 2: Validation and Intercomparison

Kai Yan [1,2], Taejin Park [2], Guangjian Yan [1,*], Zhao Liu [2], Bin Yang [2,3], Chi Chen [2], Ramakrishna R. Nemani [4], Yuri Knyazikhin [2] and Ranga B. Myneni [2]

1 School of Geography, State Key Laboratory of Remote Sensing Science, Beijing Normal University, Beijing 100875, China; kaiyan.earthscience@gmail.com

2 Department of Earth and Environment, Boston University, Boston, MA 02215, USA; taejin1392@gmail.com (T.P.); liuzhaofairy@gmail.com (Z.L.); ybjason@bu.edu (B.Y.); chenchi@bu.edu (C.C.); jknjazi@bu.edu (Y.K.); ranga.myneni@gmail.com (R.B.M.)

3 Beijing Key Lab of Spatial Information Integration and Its Applications, Institute of RS and GIS, Peking University, Beijing 100871, China

4 The National Aeronautics and Space Administration (NASA) Ames Research Center, Moffett Field, CA 94035, USA; rama.nemani@nasa.gov

* Correspondence: gjyan@bnu.edu.cn; Tel.: +86-010-5880-2085

Academic Editors: Alfredo R. Huete and Prasad S. Thenkabail

Received: 4 April 2016; Accepted: 25 May 2016; Published: 30 May 2016

Abstract: The aim of this paper is to assess the latest version of the MODIS LAI/FPAR product (MOD15A2H), namely Collection 6 (C6). We comprehensively evaluate this product through three approaches: validation with field measurements, intercomparison with other LAI/FPAR products and comparison with climate variables. Comparisons between ground measurements and C6, as well as C5 LAI/FPAR indicate: (1) MODIS LAI is closer to true LAI than effective LAI; (2) the C6 product is considerably better than C5 with RMSE decreasing from 0.80 down to 0.66; (3) both C5 and C6 products overestimate FPAR over sparsely-vegetated areas. Intercomparisons with three existing global LAI/FPAR products (GLASS, CYCLOPES and GEOV1) are carried out at site, continental and global scales. MODIS and GLASS (CYCLOPES and GEOV1) agree better with each other. This is expected because the surface reflectances, from which these products were derived, were obtained from the same instrument. Considering all biome types, the RMSE of LAI (FPAR) derived from any two products ranges between 0.36 (0.05) and 0.56 (0.09). Temporal comparisons over seven sites for the 2001–2004 period indicate that all products properly capture the seasonality in different biomes, except evergreen broadleaf forests, where infrequent observations due to cloud contamination induce unrealistic variations. Thirteen years of C6 LAI, temperature and precipitation time series data are used to assess the degree of correspondence between their variations. The statistically-significant associations between C6 LAI and climate variables indicate that C6 LAI has the potential to provide reliable biophysical information about the land surface when diagnosing climate-driven vegetation responses.

Keywords: Leaf Area Index (LAI); Fraction of Photosynthetically-Active Radiation (FPAR); MODIS; Collection 6; evaluation; validation; intercomparison

1. Introduction

The Leaf Area Index (LAI) and Fraction of Photosynthetically-Active Radiation absorbed by vegetation (FPAR) are two key biophysical variables required by most global models of climate, ecosystem productivity, biogeochemistry, hydrology and ecology [1]. Satellite remote sensing is the most effective way of collecting these variables at a large scale over a long period of time on a regular basis [2]. The MODerate resolution Imaging Spectroradiometer (MODIS) instruments on

board NASA's Terra and Aqua platforms are designed for monitoring the Earth's atmosphere, ocean and land surface and started operational production and distribution of the LAI/FPAR products from 2000. These datasets are widely used as inputs for land surface models and as training data for neural-network-based LAI/FPAR products, such as GLASS and GEOV1 [3,4]. During the past sixteen years, the MODIS science team aimed to provide users with better products by updating product cohorts, which are called collections. Collection 6 (C6) represents the latest such cohort and contains the entire time series from February 2000 to the present. C6 was released and distributed free of charge to the public from August 2015 and is expected to benefit from improvements of the input data [5].

It is critical to understand the accuracy of the product in order to effectively use LAI/FPAR in land surface models [6–11]. There are several schemes to evaluate remote sensing products, including direct validation, intercomparison and other indirect approaches. Many evaluation efforts for previous collections of MODIS LAI/FPAR products can be found in the literature from both the MODIS science team and interested users [9–13]. Special attention has been paid to the accuracy of the estimates, improvements in a new version and consistency with other global products. Collection 5 (C5) products were found to benefit from refinements of algorithm and input data [9]. Intercomparisons with other global products suggested that C5 products are reliable and consistent [8,11]. The main drawbacks of C5 LAI/FPAR were reported to be unrealistically strong temporal variability and systematic overestimation of FPAR over sparsely-vegetated areas [8].

The recently released C6 products have not been validated with ground measurements or compared to existing global products. Thus, it is critical to evaluate the new products, as users are advised to switch to C6. In this context, the primary objectives of this paper are to evaluate the MODIS LAI/FPAR C6 products and to investigate the differences between MODIS products and other global products. This is achieved comprehensively through three approaches: (1) direct validation with ground measurements; (2) intercomparison with GLASS, CYCLOPES and GEOV1 products; and (3) comparison with climate variables.

This paper is organized as follows. Section 2 provides a general description of the datasets used in this study, including global LAI/FPAR products, validation sites and time series of climate variables. Section 3 details three approaches used for validating and intercomparing the LAI/FPAR products. Results and discussion from the various evaluation analyses are documented in Section 4. Concluding remarks are presented in Section 5.

2. Datasets

2.1. Global LAI/FPAR Products

In this section, the main characteristics of the remotely-sensed global LAI/FPAR products under study are described. A brief summary of these characteristics is given in Table 1.

2.1.1. MODIS LAI/FPAR

As described in [2,14], the main algorithm generating the MODIS LAI/FPAR products is based on a three-Dimensional Radiative Transfer (3D RT) model in which atmospherically-corrected reflectances observed by the MODIS instrument and a biome map are used to generate the retrievals. Given daily land surface Bi-directional Reflectance Factors (BRFs) and their uncertainties, the algorithm finds the best LAI and FPAR estimates from biome-specific Look-Up-Tables (LUTs). A back-up empirical method based on the relationships between the Normalized Difference Vegetation Index (NDVI) and LAI/FPAR are utilized to produce estimates with relatively poor quality. LAI and FPAR are produced daily. The LAI value corresponding to the maximum FPAR is selected over the four-day or eight-day compositing period. Vegetation clumping is accounted for at the plant and canopy scales through the model. Therefore, the LAI corresponds to true LAI in all biomes. However, in the case of needle-leaf forest, shoot clumping is not accounted for. The FPAR is defined as the instantaneous black-sky value

at the time of the Terra overpass (10:30 a.m.). MODIS products store the corresponding Quality Control (QC) data layers, and the users are advised to consult the quality flags when using these products.

C6 represents the latest version of MODIS LAI/FPAR [5]. The most important change in C6 is that products are being produced at 500-m spatial resolution instead of 1 km, as in C5. A new version of MODIS surface reflectances (MOD09GA C6) is used to replace the previous used 1-km intermediate dataset (MODAGAGG). C6 also replaces the 1-km static land cover input with new multi-year land cover maps at 500-m resolution. From a consistency check of C6 with C5 [5], there are no significant discrepancies between the two collections in terms of global distributions, seasonal variations, interannual LAI anomalies and the spatial coverage of high quality retrievals. A simulation experiment suggested that the differences caused by scale effects are negligible for FPAR and low in the case of LAI [5]. In this study, we only use data from Terra (MOD) instead of Aqua (MYD) or the combined product (MCD) for three reasons: (1) the earlier overpass time of Terra results in more successful retrievals due to low cloud contamination; (2) the GLASS, CYCLOPES and GEOV1 products have a similar acquisition time s Terra; and (3) the GLASS and GEOV1 products have partly been based on MODIS LAI/FPAR from the Terra-MODIS sensor [15].

Table 1. Global LAI/FPAR products investigated in this study. GSD, LUT, RT, GRNN, ANN, tLAI and eLAI stand for "Ground Sampling Distance", "Look-Up Table", "Radiative Transfer", "General Regression Neural Network", "Artificial Neural Network", "true LAI" and "effective LAI", respectively.

Product	GSD	Frequency	Projection	Sensor	Main Algorithm	LAI Type	Ref.
MODIS C5	1 km	8-day	SIN [4]	MODIS	LUT based on 3D RT	tLAI	[2,14]
MODIS C6	500 m	8-day	SIN	MODIS	LUT based on 3D RT	tLAI	[5]
GLASS [1] V03	1 km	8-day	SIN	MODIS	GRNN trained with CYC * and MOD [5]	tLAI	[3,16]
CYC [2] V3.1	1/112°	10-day	Plate Carrée	VGT	ANN trained with 1D RT	eLAI	[17,18]
GEOV1 [3] V1.3	1/112°	10-day	Plate Carrée	VGT	ANN trained with CYC and MOD	Fused with tLAI and eLAI	[4,8]

[1] MODIS period; [2] CYCLOPES; [3] VGT period; [4] Sinusoidal; [5] clumping-corrected CYCLOPES, "MOD" stands for "MODIS"; * stands for "CYCLOPES".

2.1.2. CYCLOPES LAI/FPAR

The CYCLOPES LAI/FPAR product (http://postel.mediasfrance.org) was produced with data from the SPOT-VGT sensor at 1/112° (about 1 km at the Equator) spatial resolution and a 10-day temporal resolution, in a Plate Carrée projection, for the period 1999–2007 [17,18]. The algorithm used the red, near-infrared and short-wave infrared reflectances, which had been normalized to a standard geometry. LAI and FPAR were estimated using a neural network trained from simulations from a coupled leaf and canopy radiative transfer model (PROSAIL [19]) without using land cover input. Clumping at the plant and canopy scales was not represented in the algorithm, but landscape clumping was represented by considering mixed pixels made of a fraction of pure vegetation and a complement fraction of pure bare soil. Therefore, the LAI corresponds to effective LAI rather than true LAI. The FPAR is defined as the instantaneous black-sky FPAR at 10:00 a.m., referring only to the green elements. The CYCLOPES product was provided with the corresponding error estimate and a quality flag. The early saturation of LAI was reported as the main drawback of the CYCLOPES product [8].

2.1.3. GLASS LAI

The Global Land Surface Satellite (GLASS) LAI dataset was generated and released by Beijing Normal University (http://www.bnu-datacenter.com) [16]. This product has a temporal resolution

of eight days and spans from 1982–2012. From 1982–1999, the product was generated from AVHRR reflectances and provided in a geographic projection at the resolution of 0.05°. From 2000–2012, the product was derived from MODIS land surface reflectance (MOD09A1) and provided in a sinusoidal projection at a resolution of 1 km for the globe. In this study, we only focus on the product during the MODIS period. GLASS LAI was derived from reprocessed MODIS reflectance data using General Regression Neural Networks (GRNNs) [3]. GRNNs were trained by a database that was generated from MODIS and clumping-corrected CYCLOPES LAI products over BELMANIP (Benchmark Land Multisite Analysis and Intercomparison of Products) sites during the period from 2001–2003. MODIS LAI and clumping-corrected CYCLOPES LAI were fused in a weighted linear combination in order to obtain the best LAI estimate as follows:

$$LAI_{fused} = \omega LAI_{mod} + (1-\omega) LAI^{*}_{cyc}, \text{ with} \quad (1)$$

$$\omega = f_{mod}/(f_{mod} + f_{cyc}) \quad (2)$$

where, LAI_{fused} is a combined estimate of LAI, LAI_{mod} is the smoothed and gap-filled MODIS LAI, LAI^{*}_{cyc} is the true LAI converted from the CYCLOPES LAI and ω is the normalized weight for the MODIS LAI. Thus, linear regressions were constructed between MODIS and CYCLOPES for each biome type. The weights for each biome were determined by the deviation of MODIS and CYCLOPES (*i.e.*, f_{mod} and f_{cyc}) from the ground-measured LAIs. A quality control layer was attached to show the processing status, the quality of inputs and contamination by snow, clouds and shadows.

2.1.4. GEOV1 LAI/FPAR

The GEOV1 LAI/FPAR is the first version of the global biophysical products under the Geoland2 project (http://www.copernicus.eu/projects/geoland2). More than 30 years (1981–present) of the global LAI and FPAR were derived from AVHRR, SPOT-VGT and PROBA-V observations during three temporal periods using neural networks. In this study, we use the product during the VGT-derived period (1998–2014). LAI and FPAR during this period were derived at 1/112° spatial resolution with a 10-day step in a Plate Carrée projection (http://land.copernicus.vgt.vito.be) [4,8]. The MODIS and CYCLOPES products were first fused to obtain the best LAI (same for FPAR) estimate as follows:

$$LAI_{fused} = \omega LAI_{mod} + (1-\omega) LAI_{cyc}, \text{ with} \quad (3)$$

$$\omega = \min(1, \frac{1}{4} LAI_{cyc}) \quad (4)$$

where LAI_{fused} is a combined estimate of LAI, LAI_{mod} is the MODIS LAI, LAI_{cyc} is the CYCLOPES LAI and ω is the weight for MODIS LAI. The weight is determined by LAI_{cyc} and a threshold value (LAI_{cyc} = 4), which corresponds to the value when CYCLOPES starts to saturate. Neural networks were trained between the fused LAI and the VGT surface directionally-normalized reflectances over BELMANIP sites without biome type specification. Once trained, these networks were run to provide LAI/FPAR every 10 days within the 30-day composite period from the VGT sensor along with quality flags and quantitative uncertainties. The GEOV1 LAI is the combination of true and effective LAI, because MODIS and CYCLOPES LAI correspond to true and effective LAI, respectively. GEOV1 FPAR corresponds to the instantaneous black-sky value around 10:15 a.m. and is calculated by selecting 70% of the cumulative FPAR distribution of daily values within the compositing period instead of the maximum FPAR, as in the case of MODIS [2].

2.2. Validation Sites and BELMANIP Network

The validation dataset is from a collection of sites for which ground measurements have been collected and processed according to the CEOS/WGCV-LPV guidelines [7,20]. An empirical "transfer function" between high spatial resolution radiometric data and the biophysical measurements was

used to scale local ground measurements up to the 3 km × 3 km area of the site. There are currently 113 such datasets available, corresponding to sites and various dates of measurements.

The BELMANIP network of sites was designed to represent the global variability of vegetation types and climatological conditions [21]. This network was mainly built using sites from existing experimental networks (FLUXNET, AERONET, VALERI, BigFoot, *etc.*) and complemented with additionally sites from the GLC2000 land cover map. The site selection was performed for each band of latitude (10° width) by keeping the same proportion of biome types within the selected sites as within the whole latitude band. Attention was paid so that the sites were homogeneous over a 10 × 10 km^2 area, almost flat and with a minimum proportion of urban area and permanent water bodies. Note that there are no ground measurements for most of these sites, and therefore, this network is always used for intercomparison, rather than direct validation. Representing the latest version, the BELMANIP2.1 currently contains 445 sites and is used in this study.

2.3. Time Series of Climate Variables

This study uses the Time Series (TS) datasets of global surface temperature and precipitation that were produced by the Climatic Research Unit (CRU) at the University of East Anglia [22]. Climate variables were calculated for each 0.5° × 0.5° latitude/longitude grid, monthly, by employing a triangulated linear interpolation method. Through the auspices of the World Meteorological Organization (WMO) in collaboration with the U.S. National Oceanographic and Atmospheric Administration (NOAA), archives provided by more than 4000 meteorological stations were used to cover the world's land areas. At present, the latest time series data (TS 3.23) were generated by the CRU for the period 1901–2014 and publicly available from http://www.cru.uea.ac.uk.

3. Methodology

3.1. Direct Validation with Ground Measurements

3.1.1. Selection of Reliable Ground Measurements

We use the spatially-averaged values over a 3 km × 3 km reference map as the "ground truth" at each validation site, as in previous studies [7,8]. However, several sources of uncertainties reduce the reliability of these measurements. First, optical instruments (e.g., LAI2000) that are generally used for point-scale measurements only provide effective LAI (eLAI), which may result in an underestimation of true LAI (tLAI) [23] up to 70% in coniferous forests [24]. Second, the scale effect in indirect ground measurement can result in obvious uncertainties when the sampling length is not properly selected and this has often been ignored [25]. Third, the up-scaling scheme using an empirical "transfer function" between high spatial resolution reflectances and point-scale biophysical measurements requires a relatively large homogenous area, which may not be satisfied at some sites. Last but not least, uncertainties can arise due to the effects of the point spread function and geo-location errors of the satellite pixel. The overall uncertainty at each site differs with vegetation type, surface homogeneity, equipment used, sampling strategy, *etc.* [26]. However, absolute uncertainties of LAI reference maps corrected for clumping and non-green elements are expected to be smaller than 1 LAI unit in most sites [27]. The uncertainty is expected to be around 0.1 for FPAR [8].

Figure 1 shows the biome type distribution within each 3 km × 3 km validation site based on the MODIS land cover product (500-m resolution, C5). The upper part of the plot denotes the information entropy of the biome type for each site. This serves as an indicator of surface homogeneity. The information entropy is calculated using the proportion of each biome type within a specific site as follows:

$$H = -\sum_{i=1}^{11} (P_i * \log_2 P_i) \quad (5)$$

where H is information entropy and P_i represents the proportion of the area covered by the i-th biome type. The value 11 corresponds to the total number of MODIS land cover types. We screened out some of the 113 sites to improve the overall accuracy of these measurements. This screening was based on four criteria: (1) Presence of 500 m × 500 m pixels labeled as "water" with the 3 km × 3 km site; (2) the information entropy of biome type was greater than 1; (3) the proportion of invalid MODIS pixels (based on QC in Table 2) was larger than 40%; and (4) suspicious LAI/FPAR values (e.g., LAI < 2 for dense forests, Site #42) based on field experience and literature reports [8].

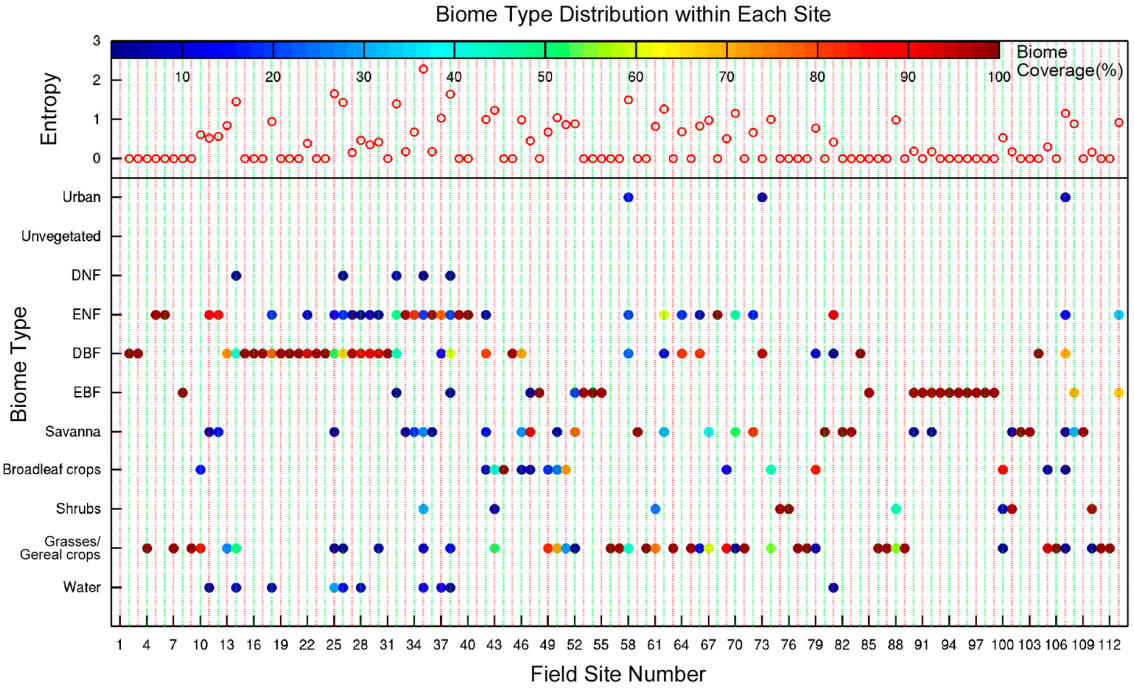

Figure 1. Biome type distribution within each 3 km × 3 km validation site based on the 500-m resolution MODIS C5 land cover product. The bottom part of the plot shows biome types and the corresponding proportion of coverage within each site. EBF, DBF, ENF and DNF stand for "Evergreen Broadleaf Forest", "Deciduous Broadleaf Forest", "Evergreen Needleleaf Forest" and "Deciduous Needleleaf Forest", respectively. The top part of the plot shows the biome type information entropy of each site calculated using Equation (5). Zero means there is only one biome type in the site or the site is a homorganic site. A larger entropy value means larger heterogeneity.

Table 2. Quality control for the four products under study.

Product	Quality Flag	Snow	Cloud	Shadow	Aerosol	Cirrus	Suspect	Overall
MODIS	FparLaiQC	Clear	Clear	-	No	No	-	-
	FparExtraQC	-	Clear	Clear	-	-	-	Good
GLASS	QC	Clear	Clear	Clear	-	-	-	Good
CYCLOPES	SM	Clear	-	-	Pure	-	No	Good
GEOV1	QFLAG	Clear	-	-	Pure	-	No	Good

3.1.2. Validation of MODIS LAI/FPAR Product

We compared both MODIS C5 and C6 products with ground measurements. The spatial and temporal mismatch between the remote sensing product and ground truth is the main issue related to such a comparison [4,18]. A 3 × 3 array of surrounding pixels has been recommended for calculating the mean value to reduce geolocation uncertainties [8]. Considering that reference maps cover a 3 km × 3 km area, which contains about 36 (6 × 6) MODIS C6 pixels and 9 (3 × 3) C5 pixels,

we averaged all of the valid pixels within the reference map. The corresponding 8-day composite, which includes the date of ground measurements was extracted. Thus, the maximum temporal mismatch is about 7 days, which should have minimal impact in most cases. Compared to the overall uncertainties of the LAI reference maps, uncertainties caused by spatial and temporal mismatch may be thus ignored. As suggested by the MODIS product user guide, the QC layers were consulted to exclude retrievals with poor quality caused by snow, clouds or high aerosol content (details in Section 3.2.1). Only retrievals from the main algorithm were used for the validation analyses reported here.

3.2. Intercomparison with Existing Global Products

3.2.1. Quality Control for Products

All of the four products under study provide QC layers, and users are advised to consult the quality flags when using them. Therefore, we performed quality control for each product using the criteria listed in Table 2. In agreement with other studies [6–8,10,18], land pixels contaminated by clouds or marked as "snow", "aerosol", "cirrus" or "suspected" according to the QC information were marked as invalid data. Note that quality control for different products was not identical because of different QC layers. For instance, MODIS and GLASS were masked by cloud, while CYCLOPES and GEOV1 were not. The MODIS biome map was used to exclude bare areas from this analysis. This study used retrievals from both the main and back-up algorithms in order to show the performance of the products instead of algorithms.

3.2.2. Comparison of Spatial Distribution

This study evaluated the four global LAI/FPAR products at the continental and global scale to characterize their performances. These products must be resampled to an identical projection and period to enable pixel-by-pixel comparisons. The four products were first quality controlled as described in Section 3.2.1 and then resampled to the Plate Carrée projection with a quarter degree spatial resolution. The LAI/FPAR values for each $0.25^\circ \times 0.25^\circ$ pixel were computed as the average of all valid native pixels falling within the coarser grid. A no-data value was assigned if more than 30 percent of the native pixels were composed of invalid data (based on QC in Table 2). The datasets with different temporal compositing periods were averaged into a monthly time step. The pixel was assigned with a no-data value if there were no valid data within the whole month.

Pixel-by-pixel absolute differences (MODIS minus other products) between MODIS and the other three LAI products and other two FPAR products were calculated and mapped at the global scale for visual comparison. Histograms of global LAI and FPAR from each product were computed and compared. Two particular months—January and July in 2001—were selected to represent the boreal winter and summer, respectively. In addition, the spatial consistency of LAI over the African continent was investigated. As in [7], we extracted and compared latitudinal LAIs from the four products along the longitudes between 20° E and 25° E.

3.2.3. Comparison at the Site Scale

We compared four LAI products and three FPAR products over 445 BELMANIP2.1 sites. Products were masked by QC flags and aggregated into a monthly time step. LAI and FPAR values from the 60 months of the 2001–2005 period were used to assess the discrepancies between different products through scatterplots. In this exercise, the original projections of the products were kept, and a 1-km (for MODIS and GLASS) or $1/112^\circ$ (for CYCLOPES and GEOV1) spatial resolution was adapted. This is because of two reasons: (1) the high homogeneity of these sites reduces the geolocation uncertainties due to different projection systems, target shift and different point spread functions [21]; and (2) any additional processing including reprojection and resampling would introduce more uncertainties [6].

The MODIS land cover map was used to divide the 445 sites into three broad vegetation classes in terms of canopy structure and leaf shape. The three classes are non-forest (Biomes 1–4), broadleaf

forests (Biomes 5 and 6) and needleleaf forests (Biomes 7 and 8). Regression equations for any two products, as well as the corresponding coefficient of determination (R^2) and root-mean-squared error (RMSE) were computed to assess the consistency.

3.2.4. Temporal Comparison

We evaluated temporal LAI/FPAR profiles of the four products extracted over seven validation sites where some ground measurements were available during the period from 2001–2004. Each site represented one vegetation type in the MODIS classification scheme. There was no validation site that could be used for DNF. Monthly LAI/FPAR estimates were first calculated using the same approach described in Section 3.2.3. Then, the seasonal variations of the four products were compared for both LAI and FPAR with R^2 and RMSE denoting the consistency.

3.3. Comparison with Climate Variables

Using independent geographic variables to explain the interannual variations of LAI/FPAR is a novel approach of indirectly evaluating these products. Due to a lack of long-term data, this evaluation method has not been used for MODIS LAI/FPAR previously. In this study, we applied this approach using thirteen years (2002–2014) of MODIS C6 LAI data. 2000 and 2001 were not included because of the missing data in these two years. The C5 and C6 LAI products were firstly resampled to the Plate Carrée projection and aggregated to a half degree spatial resolution and a monthly time step. QC information was taken into account to exclude retrievals with poor quality. In this manner, the LAI dataset matched the datasets of climate variables both spatially and temporally. Further averaging over some specific regions and over the whole year or some specific months was done to obtain the time series for statistical analyses. An area-weighted approach was used to eliminate geometrical effects. Anomalies of LAI, temperature and precipitation were computed by subtracting the thirteen-year mean from data of specific years. We calculated standardized anomalies (anomalies normalized by their standard deviations) of LAI and surface temperature during the beginning of the growing season (April and May) for four temperature-limited regions within 60°N–90°N. We also calculated standardized anomalies of annual averages of LAI and precipitation for two water-limited regions. In addition, the correlation between annual averaged LAI and annual total precipitation in the tropical latitudes (23° S–23° N) was investigated.

4. Results and Discussion

4.1. Direct Validation

4.1.1. Characteristics of Measurements

As mentioned above, the validation data used in this paper is from a collection of sites all over the world. Therefore, the method of ground measurement (e.g., destructive sampling, LAI-2000, digital hemispherical photos, TRAC, AccuPAR and allometry) may vary from site to site and from date to date. Details of these sites can be found on http://calvalportal.ceos.org/web/olive. Note that effective LAI measured by optical instruments may differ significantly from true LAI, particularly in forests [24]. These indirect measurements that have been corrected for clumping effect are also considered as true LAI in this study. Measurements without clumping correction were discarded in some studies [7,8], but were investigated separately in this study. We also compared the MODIS FPAR with ground measurements, which was seldom done in previous studies. Measurements at the same site, but different dates were considered independently.

Table 3. Biome-specific information of ground measurements after pre-selection. The numbers of ground measurements of tLAI, eLAI and FPAR for each biome are listed. The mean values and standard deviations of both ground measurements and retrievals from the C5 and C6 products are also provided (mean value ± standard deviation).

Biome Type	# of tLAI	Ground tLAI	MODIS C5 LAI	MODIS C6 LAI	# of eLAI	Ground eLAI	MODIS C5 LAI	MODIS C6 LAI	# of FPAR	Ground FPAR	MODIS C5 FPAR	MODIS C6 FPAR
B1 [1]	12	1.37 ± 1.01	1.20 ± 0.80	1.32 ± 0.85	49	0.93 ± 0.94	0.83 ± 0.50	0.94 ± 0.62	36	0.26 ± 0.24	0.32 ± 0.14	0.33 ± 0.16
B2 [2]	2	0.18 ± 0.19	0.21 ± 0.01	0.21 ± 0.01	1	0.03 ± 0.00	0.20 ± 0.00	0.20 ± 0.00	2	0.26 ± 0.34	0.28 ± 0.21	0.31 ± 0.24
B3 [3]	0	N/A	N/A	N/A	3	2.14 ± 0.75	2.09 ± 0.43	2.14 ± 0.55	0	N/A	N/A	N/A
B4 [4]	15	1.61 ± 0.55	1.43 ± 0.69	1.46 ± 0.47	15	1.26 ± 0.36	1.43 ± 0.69	1.46 ± 0.47	4	0.44 ± 0.14	0.56 ± 0.18	0.53 ± 0.15
B5 [5]	2	4.65 ± 0.39	4.44 ± 1.66	4.65 ± 0.39	2	3.27 ± 0.18	4.44 ± 1.66	4.95 ± 1.02	2	0.92 ± 0.04	0.73 ± 0.20	0.79 ± 0.10
B6 [6]	14	3.58 ± 0.40	3.77 ± 0.99	3.79 ± 0.82	7	3.78 ± 1.26	4.74 ± 1.10	4.67 ± 0.59	0	N/A	N/A	N/A
B7 [7]	9	2.69 ± 0.76	2.58 ± 1.08	2.42 ± 0.73	5	1.72 ± 0.48	2.31 ± 0.80	2.60 ± 0.97	1	0.49 ± 0.00	0.53 ± 0.00	0.61 ± 0.00
B8 [8]	0	N/A	N/A	N/A	0	N/N	N/A	N/A	0	N/A	N/A	N/A
Overall	54	2.31 ± 1.26	2.25 ± 1.46	2.28 ± 1.38	82	1.37 ± 1.21	1.49 ± 1.36	1.59 ± 1.35	45	0.31 ± 0.27	0.36 ± 0.18	0.38 ± 0.19

[1] Grasses/cereal crops; [2] shrubs; [3] broadleaf crops; [4] savanna; [5] EBF; [6] DBF; [7] ENF; [8] DNF.

Table 3 shows biome-specific information of ground measurements after pre-selection, as described in Section 3.1.1. The mean values and standard deviations of both ground measurements and retrievals from C5 and C6 products are provided. After pre-selection, there are 54 true LAI, 82 effective LAI and 45 FPAR measurements left for further analyses. Note that there are no valid true LAI and FPAR measurements for broadleaf crops, and there are no FPAR measurements for DBF. We also lack LAI and FPAR measurements for DNF. The absence of a valid ground truth suggests that more field measurements are needed in the future to further refine this assessment. Ground measurements and MODIS estimates indicate the same vegetation density sequence: broadleaf forests > needleleaf forests > savannas > grasses/cereal crops > shrubs. LAI/FPAR values extracted from the C5 and C6 products show good agreement in all vegetation types. The slight overestimation in C6 relative to C5 is due to scale effects and refinements to surface reflectances [5]. C5 shows the most obvious underestimation in savanna, which is in agreement with [28]. This issue has been mitigated by C6 to some extent. We note that MODIS LAI overestimates the ground measurements in DBF, which was also reported by [8]. As expected, effective LAIs are lower than true LAIs for all biomes due to the lack of correction for clumping. MODIS LAI estimates are found to be closer to true LAI rather than effective LAI. The largest difference between measured LAI and C5 is achieved in EBF. However, this difference is corrected in C6. Considering all biomes, measured LAI (2.31) agrees with C6 (2.28) better than with C5 (2.25). Broadleaf forests show large differences between measured effective LAI and MODIS estimates, which is due to the unneglectable clumping effects. MODIS FPAR shows overestimation in all biomes, except for EBF, where radiative signals may saturate.

4.1.2. Comparison with Ground Measurements

Figure 2a,b compares measured LAI with MODIS C5 and C6 LAI, respectively. As expected, MODIS shows better agreement with true LAI than with effective LAI. MODIS retrievals are found to systematically overestimate effective LAI measurements, especially in forests, which agrees with Stenberg *et al.* [29], who suggested that an effective LAI can produce errors of 30%–70%. In comparison with true LAI measurements, C6 performs better than C5 with the RMSE decreasing from 0.8 down to 0.66 and R^2 increasing from 0.70–0.77. Large uncertainties are found in high LAI values, which can be explained by relatively lower algorithm accuracy due to signal saturation. Overall, most of the data are within ± 1 LAI bias, indicating that the total uncertainty of this validation work is less than 1 LAI unit. Note that this uncertainty comes from both MODIS products and other sources, including the uncertainties of reference maps and mismatch in spatial and temporal domains. We also note that the distribution of the measurements is problematic with an over-representation of low values. This is expected to be solved by adding more ground measurements, especially for broadleaf crops and forests, according to the CEOS/WGCV-LPV guidelines.

In comparisons to ground measurements, MODIS FPAR performs relatively poorly compared to LAI (Figure 2c,d). The RMSE of C5 and C6 are 0.16 and 0.15, respectively. The R^2 increases from 0.68–0.74 from C5 to C6. We notice a significant overestimation of MODIS retrievals in both C5 and C6 at low FPAR values. This systematic overestimation of FPAR over sparsely-vegetated areas was reported as a main drawback of the MODIS FPAR product [8]. However, the disagreement in this study may also be due to the fact that understories are usually not taken into account in ground measurements, which will underestimate the true FPAR [15]. Overall, most data are within ± 0.2 bias with all uncertainties included.

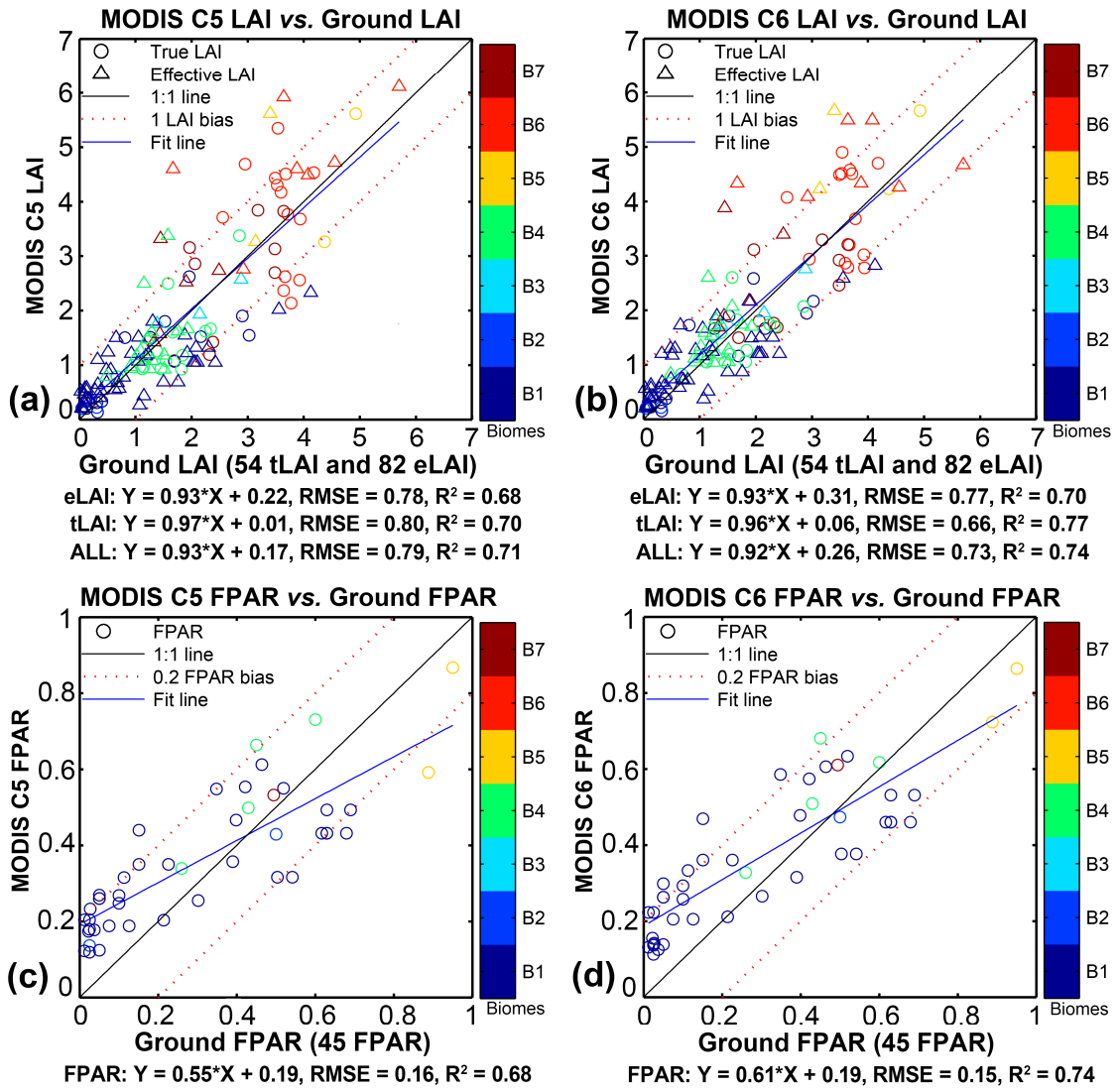

Figure 2. Comparisons between ground measured LAI (**a**,**b**) and FPAR (**c**,**d**) with MODIS C5 (left panels) and C6 (right panels) retrievals. Fifty four true LAI, 82 effective LAI and 45 FPAR measurements are used here. The 3 km × 3 km sites dominated by different biome types are depicted by different colors. Circles (triangles) in (**a**) and (**b**) represent ground LAI measurements corrected (not corrected) for clumping.

4.2. Intercomparison

4.2.1. Global LAI/FPAR Distribution

Figure 3a–c displays the global distribution of absolute LAI differences between MODIS and three other products in July 2001. Figure 3d,e shows the corresponding FPAR. As expected, the four products generally show a continuous LAI/FPAR distribution at the global scale. We notice that CYCLOPES and GEOV1 do not provide LAI or FPAR estimates at high latitudes (>74°) due to the absence of SPOT-VGT observations in these regions. South Asia and Southeast Asia are the largest regions with missing data for MODIS, CYCLOPES and GEOV1. This is caused by the frequent cloudy weather related to the southwest monsoon in these regions [30]. The reason why the GLASS product has valid data is due to gap-filling. MODIS also has missing data over the high latitudes of North America due to cloud contamination or poor atmospheric conditions.

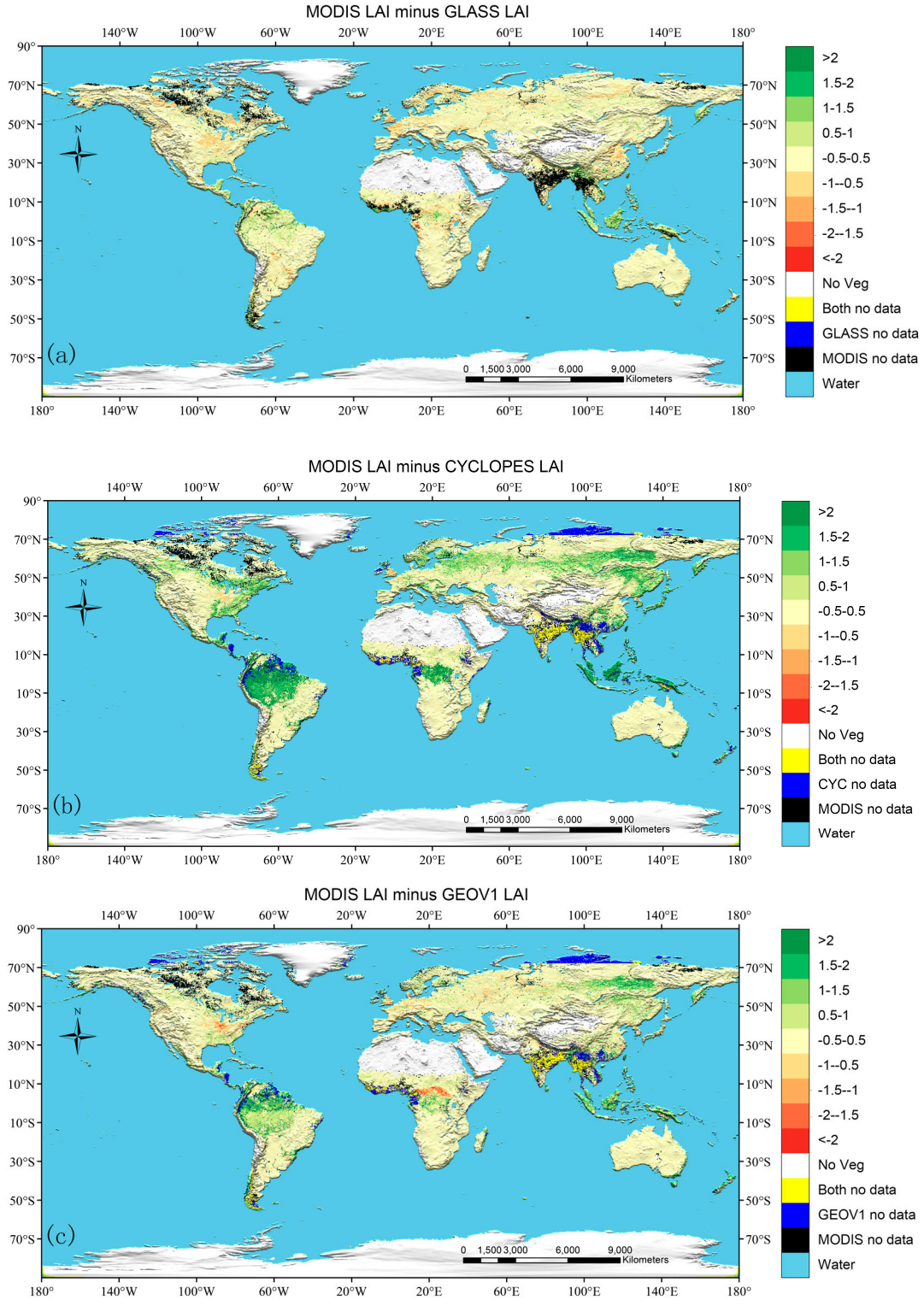

Figure 3. *Cont.*

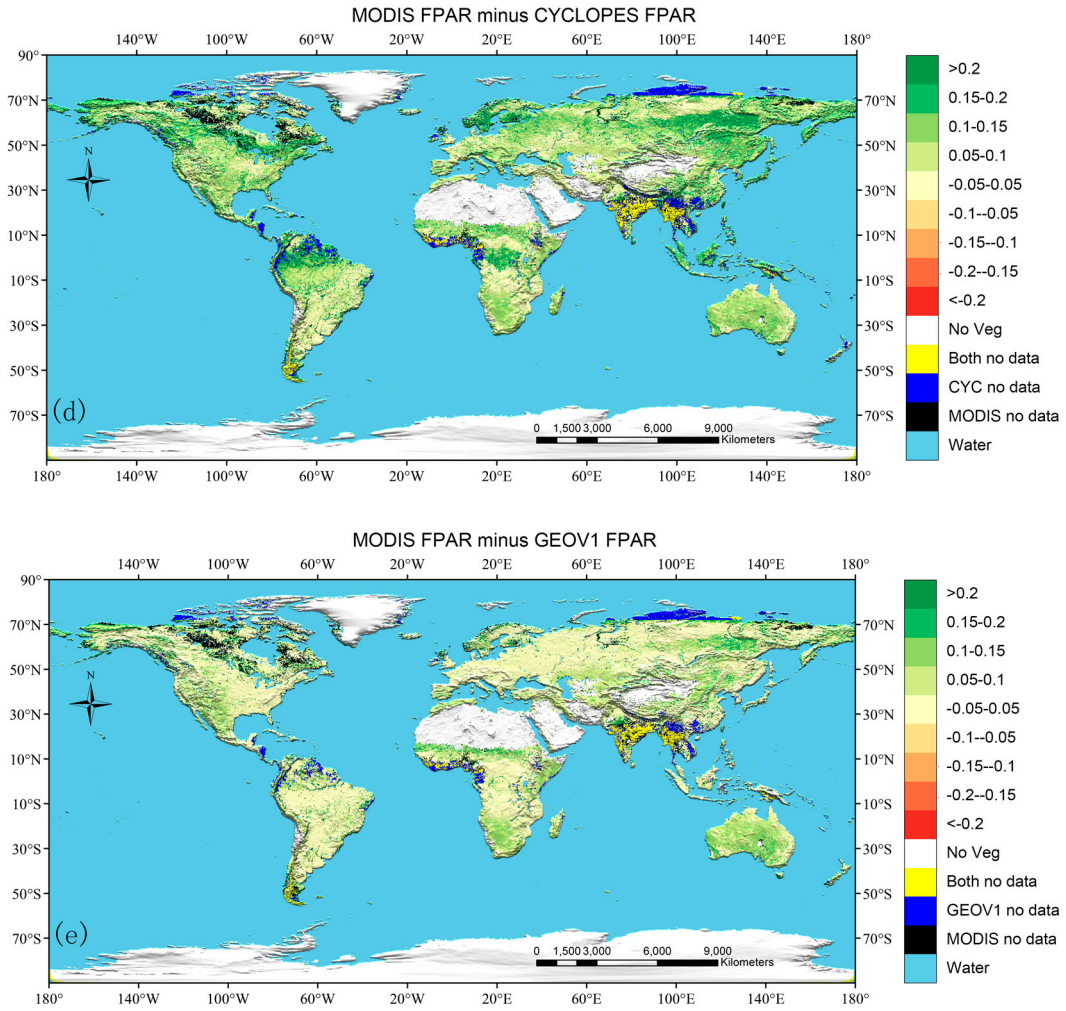

Figure 3. Global distribution of absolute differences between (**a**) MODIS and GLASS LAI; (**b**) MODIS and CYCLOPES LAI; (**c**) MODIS and GEOV1 LAI; (**d**) MODIS and CYCLOPES FPAR; and (**e**) MODIS and GEOV1 FPAR in July 2001. The spatial resolution is 0.25 degrees.

MODIS is found to agree best with GLASS, as expected, with absolute differences within $\pm$0.5 LAI units for most of the land surface (Figure 3a). The reasons are two-fold: (1) the surface reflectance data input to the two algorithms are from the same MODIS instrument; (2) MODIS LAI products are used as one part of the ANN training data for GLASS. Compared to GLASS, most overestimation of MODIS LAI is seen in tropical densely-vegetated regions. From Figure 3b,d, we notice significant underestimation from CYCLOPES, especially in densely-vegetated regions. These discrepancies between MODIS and CYCLOPES can reach to two for LAI and 0.2 for FPAR. This result agrees with previous studies and was found related to premature saturation in the CYCLPOES algorithm [7,8]. This issue was reportedly solved in GEOV1 by using the MODIS product as the training data when LAI is larger than four [4]. Indeed, we find that MODIS agrees better with GEOV1 than CYCLOPES. However, GEOV1 still shows underestimation in some regions, e.g., forests in the Amazon and South Asia. Note that the distributions of discrepancies between MODIS and GEOV1 are not consistent for LAI and FPAR.

In Figure 4a,b, the four products show smooth and consistent LAI distributions at the global scale for both January and July. Differences between global distributions are smaller in January than in July, indicating that most inconsistency occurs during the growing season of northern latitudes. The global mean LAIs calculated from MODIS, GLASS, CYCLOPES and GEOV1 are 1.42, 1.43, 1.02 and 1.15 in January and increase to 2.02, 2.09, 1.53 and 1.81 in July, respectively. Note that the number of valid

overlapping pixels also increases from 96,346 in January to 180,603 in July. This increase is caused by better atmospheric conditions and less cloud or snow contamination in the boreal summer season. Unlike other products, CYCLOPES shows a peak at around LAI = 2.5 and drops rapidly to zero after LAI = 4 in July, which confirms the early saturation issue reported previously. Compared to LAI, FPAR discrepancies are found to be relatively larger (Figure 4c,d). The global mean FPARs calculated from MODIS, CYCLOPES and GEOV1 are 0.4, 0.31 and 0.35 in January and increase to 0.54, 0.43 and 0.5 in July, respectively. The frequency of low LAI and FPAR values is considerably smaller for MODIS than for other products, which is due to the overestimation of the MODIS product in sparsely-vegetated regions [7].

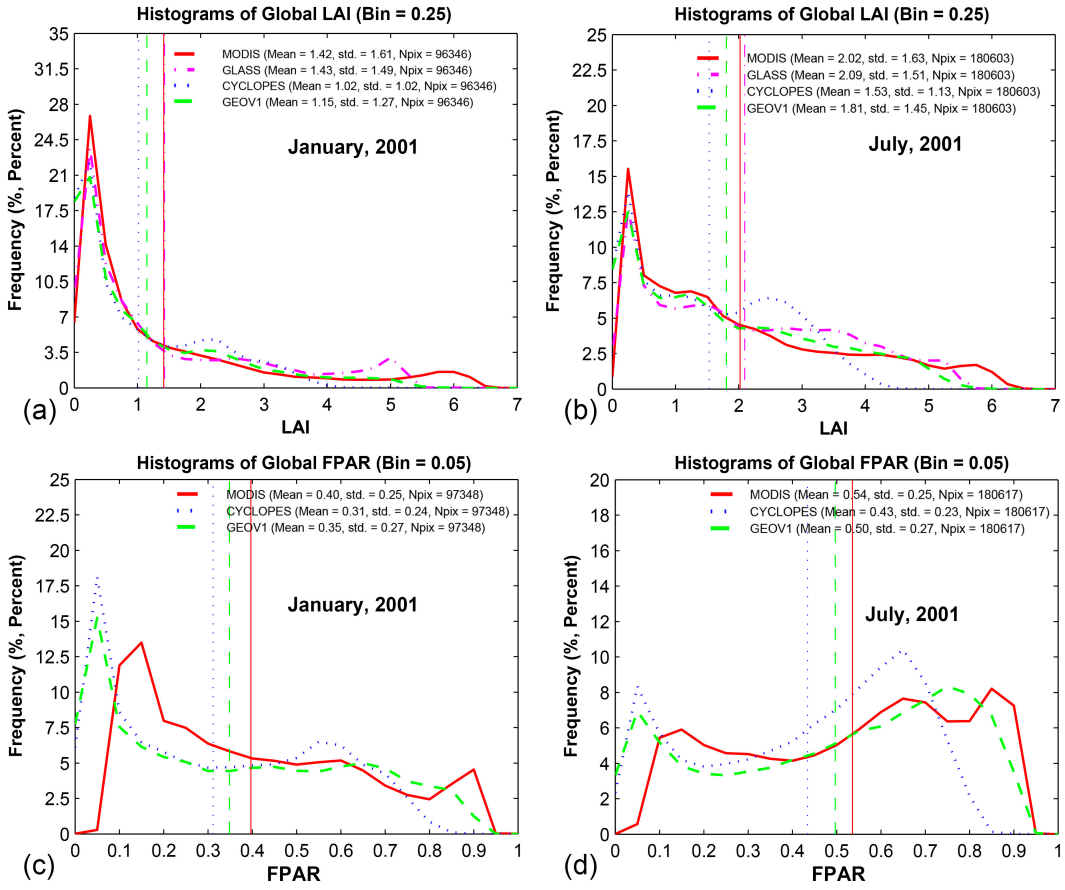

Figure 4. Histograms of global LAI (**a**,**b**) and FPAR values (**c**,**d**) from four products analyzed in this study during the months of January and July of 2001. The frequency is given as the percentage of the total number of global vegetated pixels. Global mean LAI values are depicted by vertical lines. The bins used for LAI and FPAR are 0.25 and 0.05, respectively.

4.2.2. Continental Consistency

The African continent, which is divided by the equator, was selected to assess the spatial consistency among LAIs from the four products at the continental scale. Figure 5a–c indicates that the best spatial agreement is achieved between MODIS and GLASS, with LAI differences ranging within ± 1. A significant underestimation (>2 LAI unit) is found over the central Africa forests in the case of CYCLOPES. This is somewhat alleviated in GEOV1. Missing data are not found in these annual average datasets, except in the case of MODIS near the boundaries of water bodies or barren areas.

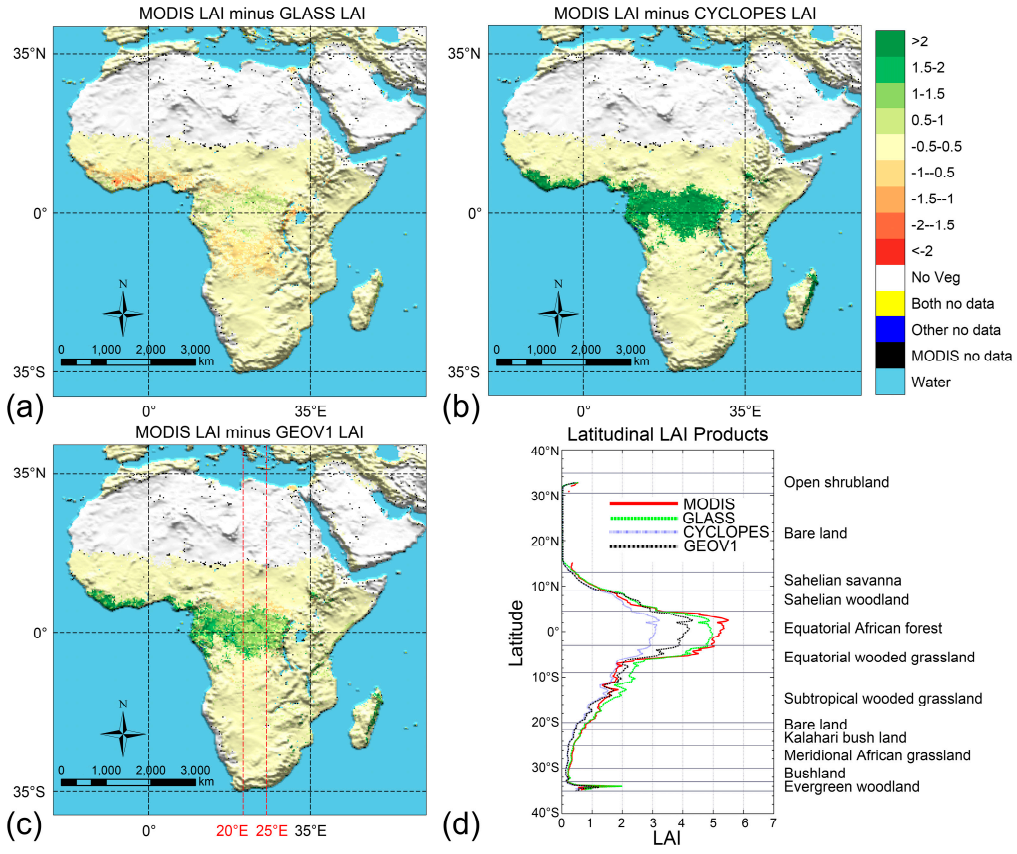

Figure 5. Comparisons of annual averaged LAI from the MODIS, GLASS, CYCLOPES and GEOV1 products over Africa in 2001. (**a**–**c**) Absolute differences between MODIS C6 and GLASS, CYCLOPES and GEOV1; (**d**) LAI from four products along the transect in Africa between 20° E and 25° E.

Figure 5d displays LAIs from MODIS, GLASS, CYCLOPES and GEOV1 along the transect within the longitude bands between 20° E and 25° E. The most obvious inconsistency is seen in equatorial forests, where LAI differences can reach one unit. CYCLOPES underestimates other products in these regions with unrealistically low LAI values. The products agree better over open shrublands and savannas. GEOV1 and CYCLOPES also show good consistency over the subtropical wooded grasslands, while GLASS overestimates them significantly. Two product groups (MODIS-GLASS and GEOV1-CYCLOPES) can be distinguished clearly over the bush lands and meridional African grasslands. This suggests that the input data sources to the algorithms play an important role in affecting the variation and magnitude of LAI/FPAR retrievals.

4.2.3. Comparison over BELMANIP Sites

Density scatter plots of monthly LAI extracted from the four products over BELMANIP2.1 sites during the period from 2001–2005 are shown in Figure 6. Results for three broad vegetation classes (non-forest, broadleaf forests and needleleaf forests) are shown separately in Table 4.

Table 4. Statistics of the intercomparisons among four LAI/FPAR products over BELMANIP sites during 2001–2005. Eight biome types are grouped into three broad categories (1–4: non-forest; 5–6: broadleaf forests; 7–8: needleleaf forests). R^2, RMSE and regression equations are provided.

Biomes		MODIS-GLASS	MODIS-CYCLOPES	MODIS-GEOV1	GLASS-CYCLOPES	GLASS-GEOV1	CYC-GEOV1
LAI	1–4	0.82/0.41/y = 1.03x + 0.10	0.83/0.36/y = 0.94x − 0.01	0.81/0.42/y = 1.05x − 0.03	0.86/0.34/y = 0.85x − 0.03	0.83/0.41/y = 0.94x − 0.06	0.95/0.23/y = 1.09x − 0.01
	5–6	0.82/0.63/y = 0.66x + 1.11	0.72/0.66/y = 0.50x + 0.81	0.79/0.74/y = 0.69x + 0.73	0.77/0.59/y = 0.69x + 0.17	0.80/0.72/y = 1.03x + 0.10	0.89/0.55/y = 1.26x + 0.05
	7–8	0.63/0.62/y = 0.74x + 0.86	0.58/0.59/y = 0.65x + 0.66	0.64/0.61/y = 0.76x + 0.64	0.65/0.57/y = 0.73x + 0.25	0.70/0.60/y = 0.86x + 0.16	0.85/0.43/y = 1.07x + 0.06
	All	0.90/0.53/y = 0.83x + 0.31	0.83/0.53/y = 0.64x + 0.26	0.88/0.56/y = 0.82x + 0.19	0.89/0.44/y = 0.74x + 0.06	0.91/0.50/y = 0.95x − 0.06	0.95/0.36/y = 1.23x − 0.07
FPAR	1–4	N/A	0.89/0.07/y = 1.04x − 0.08	0.88/0.08/y = 1.17x − 0.08	N/A	N/A	0.97/0.04/y = 1.12x + 0.01
	5–6	N/A	0.75/0.08/y = 0.77x + 0.07	0.80/0.08/y = 0.88x + 0.09	N/A	N/A	0.93/0.05/y = 1.06x + 0.06
	7–8	N/A	0.53/0.10/y = 0.75x + 0.09	0.59/0.10/y = 0.82x + 0.12	N/A	N/A	0.82/0.07/y = 0.93x + 0.11
	All	N/A	0.91/0.08/y = 0.95x − 0.05	0.91/0.09/y = 1.08x − 0.05	N/A	N/A	0.97/0.05/y = 1.12x + 0.01

Figure 6a–c shows comparisons over non-forest sites where the best agreements between any two products are observed. LAI values over these sites range from 0–2. Within this range, reflectances are not saturated, and the respective algorithms perform well. Regression lines are close to the 1:1 line with R^2 better than 0.81 and RMSE smaller than 0.42 (LAI) and 0.08 (FPAR) in all cases. This result satisfies the target accuracy (±0.5 LAI unit) expected by the Global Climate Observation System (GCOS) [31]. MODIS seems to underestimate GLASS and GEOV1, but slightly overestimates CYCLOPES. Minimum bias (R^2 = 0.95, RMSE = 0.23) is achieved between CYCLOPES and GEOV1.

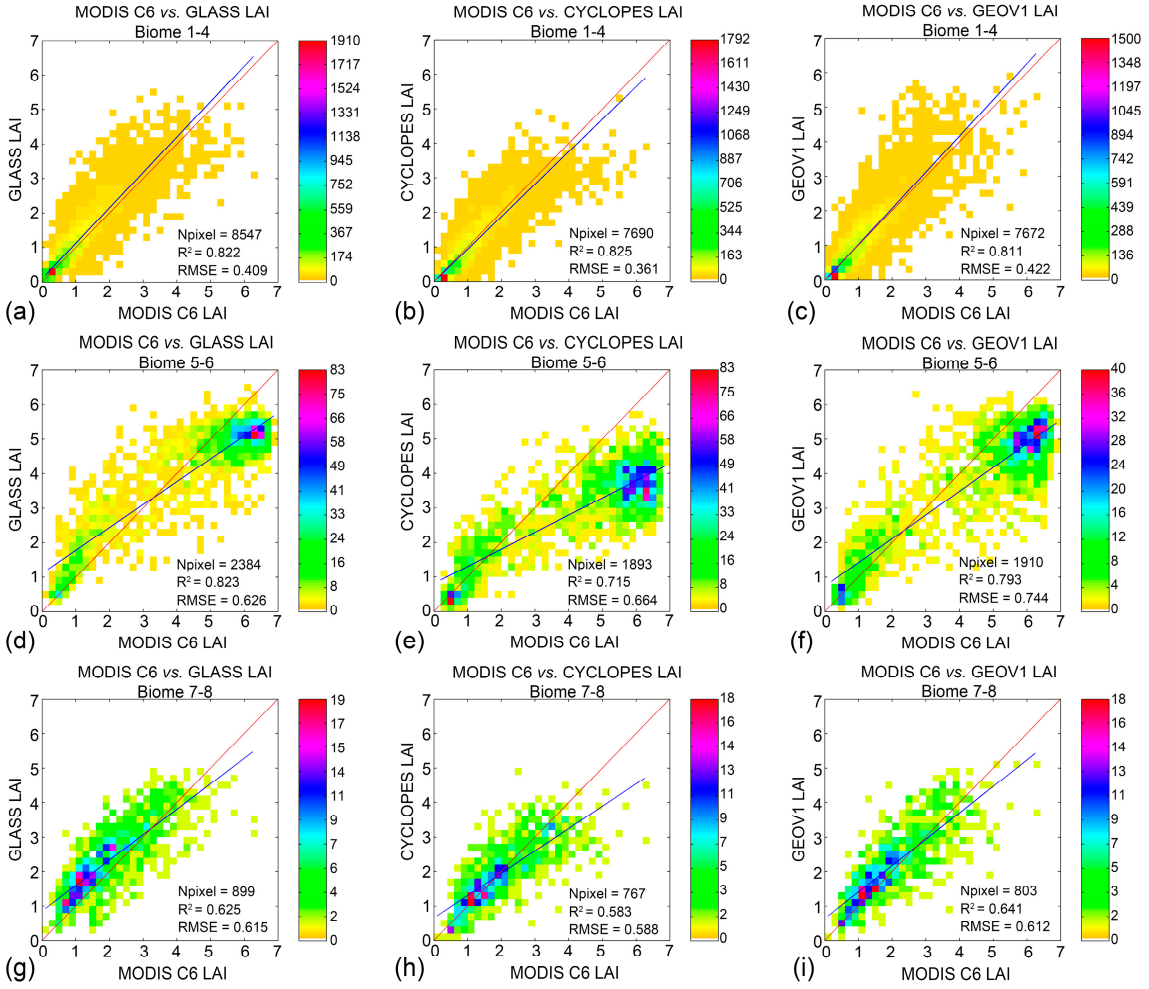

Figure 6. Density scatter plots of monthly MODIS LAI and three other LAI products (left: GLASS; middle: CYCLOPES; right: GEOV1) over BELMANIP sites during the time period from 2001–2005. The plots show a correlation between MODIS and other products for non-forest ((**a**–**c**) Biomes 1–4) in the first row, broadleaf forests ((**d**–**f**) Biomes 5 and 6) in the second row and needle leaf forests ((**g**–**i**) Biomes 7 and 8) in the third row. The red lines and blue lines are the 1:1 lines and regression lines derived from the scatter plots, respectively.

Figure 6d–f shows the case for broadleaf forests where the largest discrepancies are observed. The largest RMSE (0.74) is seen in the MODIS *versus* GEOV1 comparison and the smallest (0.55) between CYCLOPES and GEOV1. The plots show an interesting pattern where the data are in two clusters, which may be due to the monthly temporal resolution in this analysis resulting in missing some parts of the seasonality of deciduous forests. MODIS tends to underestimate in the low-LAI domain and overestimate in the high-LAI domain, relative to other products.

Similar comparisons over needleleaf forests are shown in Figure 6g–i. The total number of observations is less than 900, and this may result in additional uncertainties. CYCLOPES and GEOV1 agree well in terms of R^2 (0.85 for LAI and 0.82 for FPAR) and minimum RMSE (0.43 for LAI and 0.07 for FPAR). The discrepancies between MODIS and other products are similar with R^2 around 0.6. A slight underestimation can be noticed for MODIS at low values, especially compared to GLASS.

When considering all biome types, the RMSE of LAI (FPAR) derived from any two products ranges from 0.36 (0.05)–0.56 (0.09). The sequence from best to worst agreement is: CYCLOPES-GEOV1, GLASS-CYCLOPES, GLASS-GEOV1, MODIS-GLASS, MODIS-CYCLOPES and MODIS-GEOV1.

4.2.4. Temporal Comparison

Temporal Continuity

In the time series of LAI/FPAR products, there would be some gaps (missing data) mainly due to cloud or snow contamination, poor atmospheric conditions or technical problems, which will limit their use in land surface models [7,8]. Here, we define the "annual missing data rate" as the percent of months without valid data during the whole year. It represents the fraction in time of missing data. Note that the quality control applied for different products could be an important factor affecting this criterion.

The four lines in the upper part of Figure 7 represent variations of missing data for MODIS, GLASS, CYCLOPES and GEOV1 through four years (2001–2004). Missing data are also indicated by gaps in the LAI/FPAR time series. The missing data rate ranges from 0%–40% (five months of no data) over the seven sites. Most missing data are in the winter season, which is related to cloudiness, snow and poor atmospheric conditions, especially for high latitude sites. Sites with shrubs, broadleaf crops, savannas and broadleaf forests show low missing data rates (<20%). The four products exhibit different behaviors over different sites, and no clear conclusions can be drawn. GLASS tends to have low missing data, which may be due to a gap-filling procedure in its algorithm. GEOV1 shows a similar missing data rate as CYCLOPES, which may be expected, as both products use the same preprocessed SPOT-VGT data. MODIS shows a moderate missing data rate for most sites, which is not in agreement with some other studies [8]. This may be because our study is based on a normalized monthly temporal step instead of the native temporal resolution of each product. In addition, quality control procedures applied to the different products also affect the number of valid data in the time series.

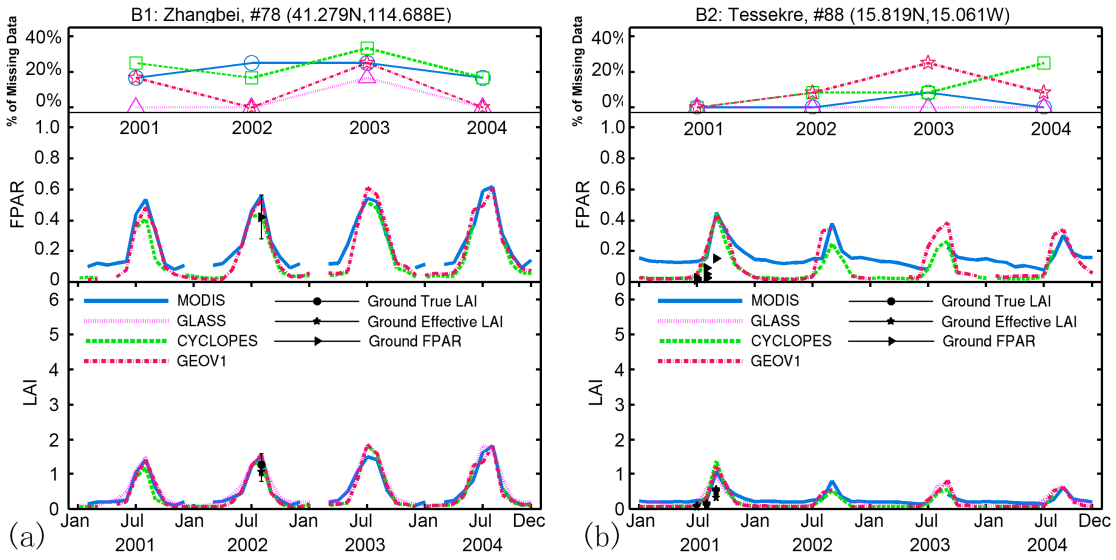

Figure 7. *Cont.*

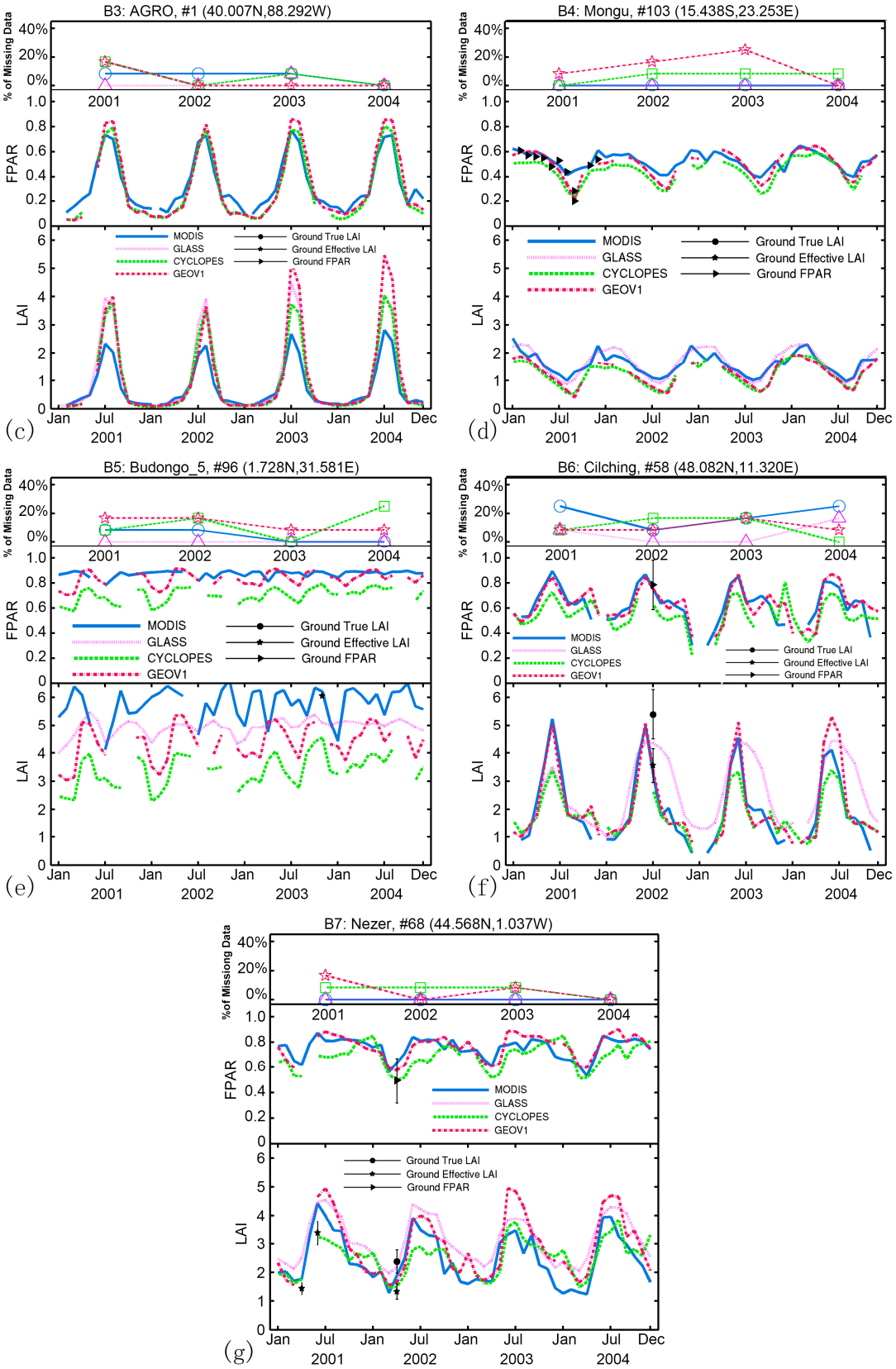

Figure 7. Temporal comparisons of LAI and FPAR among MODIS C6, GLASS, CYCLOPES and GEOV1 products over seven validation sites. Monthly averaged LAI and FAPR values for the time period from 2001–2004 are shown here. Circles, stars and triangles represent ground measurements of true LAI, effective LAI and FPAR, respectively. The four lines plotted at the top represent variations in missing data in each year. (**a**) Grasses; (**b**) shrubs; (**c**) broadleaf crops; (**d**) savanna; (**e**) EBF; (**f**) DBF; and (**g**) ENF.

Temporal Consistency

The consistency of the temporal trajectory of each product over seven validation sites for the period from 2001–2004 is discussed in this section (Figure 7). All available ground measurements are plotted in these figures as a reference. Statistics (R^2 and RMSE) of these temporal comparisons are given in Table 5.

The four products show smooth and consistent annual variations in the case of the Zhangbei grassland site in China, with some gaps in the winter season that may be due to snow contamination (Figure 7a). LAI and FPAR exhibit bell-shaped profiles, with LAI ranging from almost zero in winter to more than one in summer and FPAR ranging from 0–0.5. CYCLOPES displays systematic underestimation, as documented previously [8]. MODIS C6 is still found to systematically overestimate FPAR in sparse canopies, a problem also seen in C5 [15].

All of the products achieve good temporal continuity in shrubs (Figure 7b). LAI and FPAR are relatively low, as rainfall is limited over this site. GLASS, CYCLOPES and GEOV1 agree well, especially at low values of LAI and FPAR. MODIS shows a generally different seasonal profile, which may be realistic [32]. We find that all products overestimate both LAI and FPAR ground measurements.

Figure 7c shows the temporal variations of broadleaf crops over the AGRO site. This site shows similar temporal variations as the Zhangbei site, being about the same latitude, but there are differences in magnitude. LAI and FPAR values can reach four and 0.8, respectively. GLASS, CYCLOPE and GEOV1 agree with each other well, especially in the years 2001 and 2002. However, MODIS shows an underestimation for LAI during the growing season and overestimation of FPAR in the winter season. The LAI difference between MODIS and GEOV1 is larger than two in 2003.

The savanna site shows a different pattern of seasonality as compared to grasses, shrubs and broadleaf crops (Figure 7d). The seasonality is relatively damped with LAI values ranging from 0.5–2. The four products show similar LAI/FAPR variations and agree with ground measurements well. MODIS has no missing data during the four years.

The consistency between the four products is the worst over the EBF site (Figure 7e). This site is in Budongo rainforests where the dry season only spans from December–February and June/July. The field campaign conducted in October/November 2005 reported that LAI varies between 5.19 and 10.47 [33]. However, no clear seasonality is captured by any of the products from LAI or FPAR with high missing data rate. Similar results were reported by other studies [7,8]. This can be explained by the poor quality of satellite products due to cloud contamination and poor atmospheric conditions. The ground measurement in 2003 shows good agreement with MODIS LAI.

Figure 7f shows the case for a DBF site located in the northern high latitude. GEOV1 and MODIS agree best and are the closest to ground measurements for both LAI and FPAR in 2002. As expected, CYCLOPES underestimates all of the other products because of a lack of correction for clumping effects. Compared to others, GLASS shows artifacts related to smoothing and/or gap-filling procedures.

The four products show very similar seasonality over the ENF site (Figure 7g). LAI at this site ranges from 1–5. Thus, saturation effects are prominently seen in CYCLOPES. The MODIS profiles are noisier due to the sensitivity of retrievals to noise in reflectances at high values of LAI [7]. All products generally agree with available ground measurements. We note that CYCLOPES is closer to effective LAI measurements that is smaller than true LAI due to clumping effects.

Table 5 shows the statistical results from temporal comparisons among the four LAI/FPAR products over the seven sites during 2001–2004. R^2 and RMSE are provided as indicators of consistency. The best agreement among four products is seen in the grasses (B1) and broadleaf crops (B3) sites, with R^2 better than 0.9. The agreement between MODIS and other products is least over the EBF (B5) site. Over this site, the RMSE between MODIS and CYCLOPES is 2.56 and 0.19 for LAI and FPAR, respectively. Lager RMSE values over densely-vegetated sites (B4–B7) are observed between CYCLOPES and other products, which is due to premature saturation in the CYCLOPES algorithm [8]. Overall, MODIS agrees best with GLASS, and CYCLOPES agrees best with GEOV1. This is not surprising, as these pairs of products have the same underlying reflectances.

Table 5. Statistics of temporal comparisons among four LAI/FPAR products over seven validation sites during 2001–2004. R^2 and RMSE are provided. Values out of and in blankets are for LAI and FPAR, respectively.

Site and Biome	MODIS-GLASS		MODIS-CYC		MODIS-GEOV1		GLASS-CYC		GLASS-GEOV1		CYCLOPES-GEOV1	
	R^2	RMSE	R^2	RMSE	R^2	RMSE	R^2	RMSE	R^2	RMSE	R^2	RMSE
#78:B1	0.96	0.14	0.91(0.91)	0.17(0.09)	0.94(0.93)	0.15(0.07)	0.95	0.16	0.94	0.17	0.97(0.97)	0.10(0.05)
#88:B2	0.65	0.12	0.61(0.69)	0.20(0.11)	0.76(0.60)	0.16(0.10)	0.82	0.11	0.87	0.10	0.86(0.88)	0.10(0.06)
#1:B3	0.98	0.66	0.96(0.96)	0.62(0.08)	0.93(0.94)	0.95(0.10)	0.98	0.20	0.94	0.39	0.95(0.98)	0.45(0.05)
#103:B4	0.84	0.21	0.75(0.72)	0.42(0.10)	0.79(0.80)	0.40(0.06)	0.89	0.42	0.90	0.38	0.96(0.95)	0.1(0.06)
#96:B5	0.08	1.01	0.01(0.00)	2.56(0.19)	0.00(0.00)	1.70(0.08)	0.53	1.61	0.45	0.76	0.81(0.80)	1.01(0.13)
#58:B6	0.54	1.12	0.89(0.66)	0.57(0.12)	0.86(0.66)	0.56(0.08)	0.50	1.15	0.48	1.12	0.91(0.76)	0.74(0.10)
#68:B7	0.89	0.72	0.45(0.34)	0.69(0.12)	0.74(0.64)	0.68(0.06)	0.57	0.81	0.83	0.53	0.76(0.58)	0.74(0.11)

4.3. Evaluation with Climate Variables

Spatial and temporal variations of biophysical variables can be assessed for consistency with changes observed in meteorological fields. Several studies have focused on the relationship between the temporal variation of LAI and climate variables that govern plant growth in particular regions. From these studies, obvious correlation between LAI and precipitation in tropical regions and temperature in high latitudes regions have been reported [7,11,34,35]. In this section, we discuss the correlation between C6 LAI and temperature in northern latitudes and precipitation in some ENSO (El Niño-Southern Oscillation)-affected regions.

4.3.1. LAI Variation with Surface Temperature

Here, we present interannual variations of C6 LAI and assess their correlation to surface temperature, which can be helpful in verifying the variations in the LAI product. The spatial (60° N–90° N) and temporal (April and May) averages of standardized anomalies of LAI and surface temperature are shown in Figure 8a,b for forests and tundra, respectively. The greening trend in Eurasia was reported to be more obvious than in North America [36]. Therefore, the analysis was done separately for these two continents.

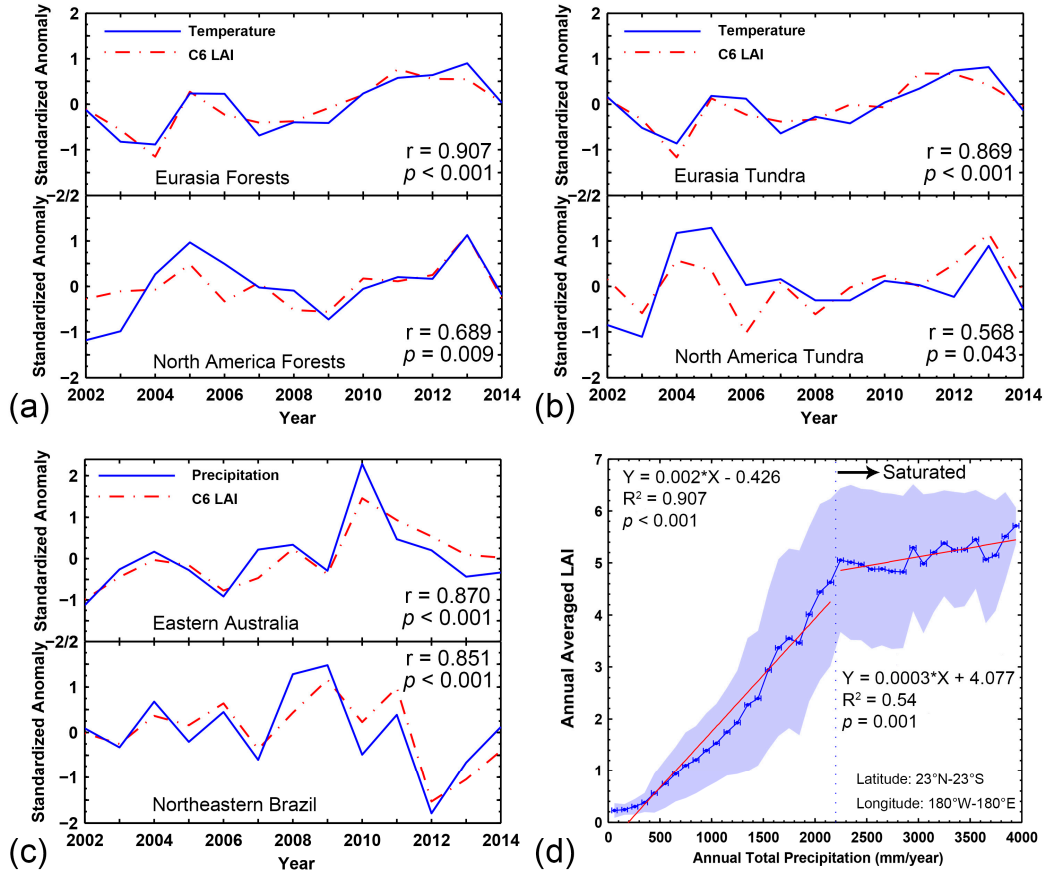

Figure 8. Evaluation of the MODIS LAI C6 product with temperature in the northern latitudes and precipitation in the ENSO-affected regions. (**a**) Temporal variations of the standardized anomalies of the growing season start period (April and May) averages of LAI and temperature for forest pixels in the northern latitudes; (**b**) same as (**a**), but for tundra pixels; (**c**) temporal variations of the standardized anomalies of annual summed LAI and precipitation in eastern Australia (20° S–40° S, 145° E–155° E) and northeastern Brazil (3° S–12° S, 35° W–45° W); (**d**) correlation between annual averaged LAI and annual total precipitation in the tropical latitudes (23° S–23° N). Standard deviations of LAIs and precipitations are denoted by blue shadow and horizontal error bars, respectively.

The anomaly time series of surface temperature and LAI correlate remarkably well, especially in Eurasian forests with a 0.907 correlation coefficient. The linkage is stronger in Eurasia than in North America. This is because North American boreal forests have experienced declining photosynthetic activity due to recent warming-induced drought, wild fires and pest infestations [37]. Our results also indicate that correlations in tundra are considerably weaker than in forests. This could be due to fewer valid data over tundra resulting from poor Sun-sensor geometry and illumination conditions. Nevertheless, we observe a slight warming and greening trend in Eurasian forests (p = 0.033 in a Mann–Kendall trend test [38]). However, no statistically-significant trend is found in tundra or North American forests ($p > 0.1$), which agrees with [11,35].

4.3.2. LAI Variation with Precipitation

The standardized anomalies of thirteen years of LAI and precipitation in two semiarid regions are shown in Figure 8c. Significant coherence between LAI and rainfall anomalies are found in both eastern Australia (r = 0.87, $p < 0.001$) and northeastern Brazil (r = 0.851, $p < 0.001$). We do not find particular directional changes in precipitation or vegetation greenness in these two regions during the period of our study. However, the high precipitation events leading to damaging Australian floods in 2010–2011 [39] are obvious with a peak in both precipitation and LAI variations. Moreover, we notice a severe drought with corresponding vegetation browning occurring in northeastern Brazil in 2012, which has been confirmed in [40].

Figure 8d shows the correlation between annual averaged LAI and annual total precipitation in the tropical latitudes (23° S–23° N). Note that this analysis was not for a specific year, but for the average of thirteen years. The precipitation range (0–4000 mm/year) was divided into 40 intervals. The mean and standard deviation of annual averaged LAI in each of the 40 precipitation bins were first computed for each of the thirteen years and then averaged over the thirteen years. We find a highly significant correlation (R^2 = 0.97, $p < 0.001$) between the two variables when precipitation is less than 2200 mm/year from where this relationship turns to saturated. Large standard deviations of LAI within each precipitation interval indicate the role of other factors in governing plant growth [35].

5. Conclusions

The objective of this paper is to evaluate the newly-released MODIS LAI/FPAR C6 product (MOD15A2H). This is achieved comprehensively through three independent approaches: validation with ground measurements, intercomparison with other satellite products and comparison with climate variables. Fifty four true LAI, 82 effective LAI and 45 FPAR ground measurements with high reliability extracted from 113 sites were used to validate the C6 and C5 LAI/FPAR products. The results showed that MODIS LAI is closer to true LAI, rather than effective LAI, due to the clumping correction in the algorithm. We found that MODIS C6 performed considerably better than C5 in comparisons to true LAI measurements. The RMSE decreased from 0.80 down to 0.66, which is close to the target accuracy ($\pm$0.5) as required by the GCOS. Both C5 and C6 showed an overestimation of FPAR over sparsely-vegetated areas, as noted previously in other studies.

Intercomparisons with three other satellite products (GLASS, CYCLOPES and GEOV1) were carried out at the site, continental and global scales to investigate the differences. The four products showed similar spatial distributions of LAI and FPAR in both January and July. MODIS and GLASS (CYCLOPES and GEOV1) were found to achieve the best agreement, most likely because the surface reflectances used as inputs to the respective algorithms were acquired from the same instrument. CYCLOPES underestimated LAI and FPAR systematically due to the lack of correction for clumping effects and premature saturation. Temporal comparisons for the 2001–2004 period indicated that the products properly captured the seasonality of different biomes, except in EBF, where the poor quality of satellite products resulted in erratic and unrealistic seasonal profiles. The four products showed different performances at different sites in terms of missing data, and no clear conclusion could be drawn.

To further imbue confidence in the LAI product, we assessed correlations between the variations of satellite-derived LAI and station-measured temperature and precipitation data over a thirteen year period. Statistically-significant agreements between these data series indicated that the interannual variations in LAI are not an artifact of remote sensing data or the algorithm.

The research presented here is critical for the further understanding and proper use of C6 LAI/FPAR products in land surface models. Furthermore, the validation and intercomparison approaches presented in this work can be used for the evaluation of similar products in the future.

Acknowledgments: Help from MODIS and VIIRS Science team members is gratefully acknowledged. This work is supported by the MODIS program of NASA and partially funded by the National Basic Research Program of China (Grant No. 2013CB733402) and the key program of NSFC (Grant No. 41331171). Kai Yan gives thanks for the scholarship from the China Scholarship Council.

Author Contributions: Kai Yan, Guangjian Yan, Yuri Knyazikhin, Ramakrishna R. Nemani and Ranga B. Myneni conceived of and designed the experiments. Taejin Park and Kai Yan performed the experiments. Taejin Park and Bin Yang analyzed the data. Zhao Liu and Chi Chen contributed to the Sections 3.3 and 4.3. All authors contributed to the writing of the paper.

Conflicts of Interest: The authors declare no conflict of interest. The founding sponsors had no role in the design of the study; in the collection, analyses or interpretation of the data; in the writing of the manuscript; nor in the decision to publish the results.

Abbreviations

The following abbreviations are used in this manuscript:

MODIS	Moderate Resolution Imaging Spectroradiometer
LAI	Leaf Area Index
FPAR	Fraction of Photosynthetically-Active Radiation
C5	Collection 5
C6	Collection 6
RT	Radiative Transfer
LUT	Look-Up-Table
BRF	Bi-directional Reflectance Factors
NDVI	Normalized Difference Vegetation Index
GSD	Ground Sampling Distance
ANN	Artificial Neural Network
GRNN	General Regression Neural Network
tLAI	True LAI
eLAI	Effective LAI
QC	Quality Control
GLASS	Global Land Surface Satellite
BELMANIP	Benchmark Land Multisite Analysis and Intercomparison of Products
TS	Time Series
CRU	Climatic Research Unit
WMO	World Meteorological Organization
NOAA	National Oceanographic and Atmospheric Administration
NASA	National Aeronautics and Space Administration
EBF	Evergreen Broadleaf Forest
DBF	Deciduous Broadleaf Forest
ENF	Evergreen Needleleaf Forest
DNF	Deciduous Needleleaf Forest
ENSO	El Niño-Southern Oscillation

References

1. Sellers, P.J.; Dickinson, R.E.; Randall, D.A.; Betts, A.K.; Hall, F.G.; Berry, J.A.; Collatz, G.J.; Denning, A.S.; Mooney, H.A.; Nobre, C.A. Modeling the exchanges of energy, water, and carbon between continents and the atmosphere. *Science* **1997**, *275*, 502–509. [CrossRef]
2. Myneni, R.B.; Smith, G.R.; Lotsch, A.; Friedl, M.; Morisette, J.T.; Votava, P.Ô.N.R.; Running, S.W.; Hoffman, S.; Knyazikhin, Y.; Privette, J.L.; *et al.* Global products of vegetation leaf area and fraction absorbed PAR from year one of MODIS data. *Remote Sens. Environ.* **2002**, *83*, 214–231. [CrossRef]

3. Xiao, Z.; Liang, S.; Wang, J.; Chen, P.; Yin, X.; Zhang, L.; Song, J. Use of general regression neural networks for generating the GLASS leaf area index product from time-series MODIS surface reflectance. *IEEE Trans. Geosci. Remote Sens.* **2014**, *52*, 209–223. [CrossRef]
4. Baret, F.; Weiss, M.; Lacaze, R.; Camacho, F.; Makhmara, H.; Pacholcyzk, P.; Smets, B. GEOV1: LAI and FAPAR essential climate variables and FCOVER global time series capitalizing over existing products. Part1: Principles of development and production. *Remote Sens. Environ.* **2013**, *137*, 299–309. [CrossRef]
5. Yan, K.; Park, T.; Yan, G.; Chen, C.; Yang, B.; Liu, Z.; Nemani, R.; Knyazikhin, Y.; Myneni, R. Evaluation of MODIS LAI/FPAR product Collection 6. Part 1: Consistency and improvements. *Remote Sens.* **2016**, *8*, 359. [CrossRef]
6. Fang, H.; Wei, S.; Liang, S. Validation of MODIS and CYCLOPES LAI products using global field measurement data. *Remote Sens. Environ.* **2012**, *119*, 43–54. [CrossRef]
7. Garrigues, S.; Lacaze, R.; Baret, F.; Morisette, J.T.; Weiss, M.; Nickeson, J.E.; Fernandes, R.; Plummer, S.; Shabanov, N.V.; Myneni, R.B.; *et al.* Validation and intercomparison of global Leaf Area Index products derived from remote sensing data. *J. Geophys. Res.* **2008**, *113*. [CrossRef]
8. Camacho, F.; Cernicharo, J.; Lacaze, R.; Baret, F.; Weiss, M. GEOV1: LAI, FAPAR essential climate variables and FCOVER global time series capitalizing over existing products. Part 2: Validation and intercomparison with reference products. *Remote Sens. Environ.* **2013**, *137*, 310–329. [CrossRef]
9. Yang, W.; Tan, B.; Huang, D.; Rautiainen, M.; Shabanov, N.V.; Wang, Y.; Privette, J.L.; Huemmrich, K.F.; Fensholt, R.; Sandholt, I.; *et al.* MODIS leaf area index products: From validation to algorithm improvement. *IEEE Trans. Geosci. Remote Sens.* **2006**, *44*, 1885–1898. [CrossRef]
10. Fang, H.; Jiang, C.; Li, W.; Wei, S.; Baret, F.; Chen, J.M.; Garcia-Haro, J.; Liang, S.; Liu, R.; Myneni, R.B.; *et al.* Characterization and intercomparison of global moderate resolution leaf area index (LAI) products: Analysis of climatologies and theoretical uncertainties. *J. Geophys. Res. Biogeosci.* **2013**, *118*, 529–548. [CrossRef]
11. Ganguly, S.; Samanta, A.; Schull, M.A.; Shabanov, N.V.; Milesi, C.; Nemani, R.R.; Knyazikhin, Y.; Myneni, R.B. Generating vegetation leaf area index Earth system data record from multiple sensors. Part 2: Implementation, analysis and validation. *Remote Sens. Environ.* **2008**, *112*, 4318–4332. [CrossRef]
12. Steinberg, D.C.; Goetz, S.J.; Hyer, E.J. Validation of MODIS F/sub PAR/products in boreal forests of Alaska. *IEEE Trans. Geosci. Remote Sens.* **2006**, *44*, 1818–1828. [CrossRef]
13. Tan, B.; Hu, J.; Zhang, P.; Huang, D.; Shabanov, N.; Weiss, M.; Knyazikhin, Y.; Myneni, R.B. Validation of Moderate Resolution Imaging Spectroradiometer leaf area index product in croplands of Alpilles, France. *J. Geophys. Res. Atmos.* **2005**, *110*. [CrossRef]
14. Knyazikhin, Y.; Glassy, J.; Privette, J.L.; Tian, Y.; Lotsch, A.; Zhang, Y.; Wang, Y.; Morisette, J.T.; Votava, P.; Myneni, R.B. *MODIS Leaf Area Index (LAI) and Fraction of Photosynthetically Active Radiation Absorbed by Vegetation (FPAR) Product (MOD15) Algorithm Theoretical Basis Document*; Theoretical Basis Document; NASA Goddard Space Flight Center: Greenbelt, MD, USA, 1999; p. 20771.
15. Majasalmi, T.; Rautiainen, M.; Stenberg, P.; Manninen, T. Validation of MODIS and GEOV1 fPAR Products in a Boreal Forest Site in Finland. *Remote Sens.* **2015**, *7*, 1359–1379. [CrossRef]
16. Liang, S.; Zhao, X.; Liu, S.; Yuan, W.; Cheng, X.; Xiao, Z.; Zhang, X.; Liu, Q.; Cheng, J.; Tang, H. A long-term Global LAnd Surface Satellite (GLASS) data-set for environmental studies. *Int. J. Digit. Earth* **2013**, *6*, 5–33. [CrossRef]
17. Baret, F.; Hagolle, O.; Geiger, B.; Bicheron, P.; Miras, B.; Huc, M.; Berthelot, B.; Niño, F.; Weiss, M.; Samain, O. LAI, fAPAR and fCover CYCLOPES global products derived from VEGETATION: Part 1: Principles of the algorithm. *Remote Sens. Environ.* **2007**, *110*, 275–286. [CrossRef]
18. Weiss, M.; Baret, F.; Garrigues, S.; Lacaze, R. LAI and fAPAR CYCLOPES global products derived from VEGETATION. Part 2: Validation and comparison with MODIS collection 4 products. *Remote Sens. Environ.* **2007**, *110*, 317–331. [CrossRef]
19. Jacquemoud, S.; Verhoef, W.; Baret, F.; Bacour, C.; Zarco-Tejada, P.J.; Asner, G.P.; François, C.; Ustin, S.L. PROSPECT+ SAIL models: A review of use for vegetation characterization. *Remote Sens. Environ.* **2009**, *113*, S56–S66. [CrossRef]
20. Morisette, J.T.; Baret, F.; Privette, J.L.; Myneni, R.B.; Nickeson, J.E.; Garrigues, S.; Shabanov, N.V.; Weiss, M.; Fernandes, R.; Leblanc, S.G. Validation of global moderate-resolution LAI products: A framework proposed within the CEOS land product validation subgroup. *IEEE Trans. Geosci. Remote Sens.* **2006**, *44*, 1804. [CrossRef]
21. Baret, F.; Morissette, J.T.; Fernandes, R.A.; Champeaux, J.L.; Myneni, R.B.; Chen, J.; Plummer, S.; Weiss, M.; Bacour, C.; Garrigues, S.; *et al.* Evaluation of the representativeness of networks of sites for the global validation and intercomparison of land biophysical products: Proposition of the CEOS-BELMANIP. *IEEE Trans. Geosci. Remote Sens.* **2006**, *44*, 1794–1803. [CrossRef]

22. Harris, I.; Jones, P.D.; Osborn, T.J.; Lister, D.H. Updated high-resolution grids of monthly climatic observations—The CRU TS3. 10 Dataset. *Int. J. Climatol.* **2014**, *34*, 623–642. [CrossRef]
23. Hu, R.; Yan, G.; Mu, X.; Luo, J. Indirect measurement of leaf area index on the basis of path length distribution. *Remote Sens. Environ.* **2014**, *155*, 239–247. [CrossRef]
24. Chen, J.M.; Cihlar, J. Quantifying the effect of canopy architecture on optical measurements of leaf area index using two gap size analysis methods. *IEEE Trans. Geosci. Remote Sens.* **1995**, *33*, 777–787. [CrossRef]
25. Yan, G.; Hu, R.; Wang, Y.; Ren, H.; Song, W.; Qi, J.; Chen, L. Scale Effect in Indirect Measurement of Leaf Area Index. *IEEE Trans. Geosci. Remote Sens* **2016**. [CrossRef]
26. Martínez, B.; García-Haro, F.J.; Camacho-de Coca, F. Derivation of high-resolution leaf area index maps in support of validation activities: Application to the cropland Barrax site. *Agric. For. Meteorol.* **2009**, *149*, 130–145. [CrossRef]
27. Fernandes, R.; Butson, C.; Leblanc, S.; Latifovic, R. Landsat-5 TM and Landsat-7 ETM+ based accuracy assessment of leaf area index products for Canada derived from SPOT-4 VEGETATION data. *Can. J. Remote Sens.* **2003**, *29*, 241–258. [CrossRef]
28. Mayr, M.; Samimi, C. Comparing the dry season *in-situ* Leaf Area Index (LAI) derived from high-resolution rapideye imagery with MODIS LAI in a namibian Savanna. *Remote Sens.* **2015**, *7*, 4834–4857. [CrossRef]
29. Stenberg, P. Correcting LAI-2000 estimates for the clumping of needles in shoots of conifers. *Agric. For. Meteorol.* **1996**, *79*, 1–8. [CrossRef]
30. Rajeevan, M.; Bhate, J.; Kale, J.D.; Lal, B. High resolution daily gridded rainfall data for the Indian region: Analysis of break and active monsoon spells. *Curr Sci. India* **2006**, *91*, 296–306.
31. GCOS. *Systematic Observation Requirements for Satellite-Based Products for Climate: Supplemental Details to the Satellite-Based Component of the "Implementation Plan for the Global Observing System for Climate in Support of the UNFCCC"*; GCOS: Singapore, Singapore, 2006.
32. Elmore, A.J.; Guinn, S.M.; Minsley, B.J.; Richardson, A.D. Landscape controls on the timing of spring, autumn, and growing season length in mid-Atlantic forests. *Glob. Chang. Biol.* **2012**, *18*, 656–674. [CrossRef]
33. Kraus, T.; Schmidt, M.; Dech, S.W.; Samimi, C. The potential of optical high resolution data for the assessment of leaf area index in East African rainforest ecosystems. *Int. J. Remote Sens.* **2009**, *30*, 5039–5059. [CrossRef]
34. Buermann, W. Analysis of a multiyear global vegetation leaf area index data set. *J. Geophys. Res. Atmos.* **2002**, *107*. [CrossRef]
35. Zhu, Z.; Bi, J.; Pan, Y.; Ganguly, S.; Anav, A.; Xu, L.; Samanta, A.; Piao, S.; Nemani, R.; Myneni, R. Global data sets of vegetation Leaf Area Index (LAI)3g and Fraction of Photosynthetically Active Radiation (FPAR)3g derived from Global Inventory Modeling and Mapping Studies (GIMMS) Normalized Difference Vegetation Index (NDVI3g) for the period 1981 to 2011. *Remote Sen.* **2013**, *5*, 927–948.
36. Zhou, L.; Tucker, C.J.; Kaufmann, R.K.; Slayback, D.; Shabanov, N.V.; Myneni, R.B. Variations in northern vegetation activity inferred from satellite data of vegetation index during 1981 to 1999. *J. Geophys. Res. Atmos.* **2001**, *106*, 20069–20083. [CrossRef]
37. Goetz, S.J.; Bunn, A.G.; Fiske, G.J.; Houghton, R.A. Satellite-observed photosynthetic trends across boreal North America associated with climate and fire disturbance. *Proc. Natl. Acad. Sci. USA* **2005**, *102*, 13521–13525. [CrossRef] [PubMed]
38. Yue, S.; Pilon, P.; Cavadias, G. Power of the Mann—Kendall and Spearman's rho tests for detecting monotonic trends in hydrological series. *J. Hydrol.* **2002**, *259*, 254–271. [CrossRef]
39. Boening, C.; Willis, J.K.; Landerer, F.W.; Nerem, R.S.; Fasullo, J. The 2011 La Niña: So strong, the oceans fell. *Geophys. Res. Lett.* **2012**, *39*. [CrossRef]
40. Marengo, J.A.; Alves, L.M.; Soares, W.R.; Rodriguez, D.A.; Camargo, H.; Riveros, M.P.; Pabló, A.D. Two contrasting severe seasonal extremes in tropical South America in 2012: Flood in Amazonia and drought in northeast Brazil. *J. Clim.* **2013**, *26*, 9137–9154. [CrossRef]